3-2022

Development of Minimum Delta-V Trajectories to Service GEO Assets from Cislunar Space

Alexander C. Urban

DEVELOPMENT OF MINIMUM DELTA-V TRAJECTORIES TO SERVICE GEO ASSETS FROM CISLUNAR SPACE

THESIS

Alexander C. Urban, 2nd Lieutenant, USAF

AFIT-ENY-MS-15-M-315

DEPARTMENT OF THE AIR FORCE
AIR UNIVERSITY

AIR FORCE INSTITUTE OF TECHNOLOGY

Wright-Patterson Air Force Base, Ohio

AFIT-ENY-MS-22-M-315

DEVELOPMENT OF MINIMUM DELTA-V TRAJECTORIES TO SERVICE GEO ASSETS FROM CISLUNAR SPACE

THESIS

Presented to the Faculty

Department of Aeronautics and Astronautics

Graduate School of Engineering and Management

Air Force Institute of Technology

Air University

Air Education and Training Command

In Partial Fulfillment of the Requirements for the

Degree of Master of Science in Space Systems

Alexander C. Urban, B.S.

2nd Lieutenant, USAF

March 2022

AFIT-ENY-MS-22-M-315

DEVELOPMENT OF MINIMUM DELTA-V TRAJECTORIES TO SERVICE GEO ASSETS FROM CISLUNAR SPACE

Alexander C. Urban, B.S.

2nd Lieutenant, USAF

Committee Membership:

Dr. Bruce A. Cox, PhD
Chair

Lt Col Bryan D. Little, PhD
Co-chair

Dr. Andrew S. Keys, PhD
Member

Lt Col Kirk W. Johnson, PhD
Member

Abstract

As of October 2019, space shifted from a benign scientific domain to a "warfighting domain" equal to land, sea, or air domains. As a result of this shift in national strategic policy there is an increased interest in the *maneuver* principle of war as it relates to space assets. However, maneuvering space assets requires expenditure of fuel and thus demands either disposable assets or the repairing, refueling, and reconstitution (R3) of non-disposable assets. Recent research has shown that R3 of GEO assets can be achieved more cost effectively using propellant extracted from the natural lunar environment using in-situ resource utilization (ISRU) technologies as opposed to terrestrially launching all propellant required to fulfill the mission. This investigation explores how to minimize the ΔV costs required of a network of service vehicles traveling from cislunar space to GEO using ISRU. In this investigation the ΔV and time-of-flight (TOF) arc costs of an event-driven generalized multicommodity network flow are generated to support the creation of a dynamic R3 scheduler model. High-thrust trajectories between various inclinations of GEO, with an Earth-Moon L1 Lyapunov orbit (L1) and with a distant prograde orbit (DPO) are explored. Additionally, the effect of orbit radius on the ΔV costs of inclination changes in GEO is also investigated to determine the optimal radius for multiple R3 deliveries within GEO. It was found that there is little variation in TOF of trajectories leaving L1, but significant variation in ΔV costs—thus ΔV considerations drive the arc selection. DPO trajectories also appear to offer significant ΔV savings in comparison to L1 trajectories. Finally, in GEO, ΔV costs

of inclination changes are minimized either at GEO radius (42,164 km) or at a multiple of 1.25xGEO radius (52,705 km).

Acknowledgments

I would like to express my sincere appreciation to my research advisor, Dr. Bruce Cox, for his guidance and support throughout all the challenges and breakthroughs of this research effort. Your guidance and input made this investigation a success. I would, also, like to thank my military advisor, Lt Col Little, for his support throughout not only this investigation, but in MECH 733 as well as my many, many questions related to administrative topics and follow-on-assignment quandaries. Additionally, I would like to thank my sponsor Karl Stolleis from the Air Force Research Laboratories for both the support and latitude provided to me in this endeavor. To my colleague, business partner, and friend Tyler Gerhold, thank you for your support and friendship over the years and especially through this period of our lives. I am grateful for this experience we have shared. Finally, I would like to express my sincere gratitude to my parents George and Susan for all their support in raising me and guiding me to accomplish my goals. Thank you.

Alexander C. Urban

Aut viam inveniam aut faciam.

Table of Contents

Page

List of Figures

Page

List of Tables

Page

DEVELOPMENT OF MINIMUM DELTA-V TRAJECTORIES TO SERVICE GEO ASSETS FROM CISLUNAR SPACE

I. Introduction

1.1 Motivation

With the rise of private launch and the adoption of Cubesats, it is becoming easier to access space, causing a substantial increase in the number of satellites orbiting Earth (Fig. 1). There are currently over 7,500 satellites in orbit around the Earth, a number which is growing almost daily [1]. Among these satellites are assets critical to national security such as communications, imagery, and positioning systems. In fact, Directive 7 of the Memorandum on Space Policy published by the White House in 2021 describes the global positioning system (GPS) as "integral to United States national security, economic growth, transportation safety, and homeland security" [2]. Congestion poses a threat to these assets as it increases the chance of collision with functioning or non-functioning satellites and debris.

While space is becoming more congested it is also becoming more contested. In October 2019, a memo from Air Force Space Command's deputy commander Maj. Gen. John Shaw characterized space as a "warfighting domain". In this memo, Maj. Gen. Shaw declared the shift from a "space-situational awareness mindset of a benign environment" to a mindset of space domain awareness (SDA). SDA is defined as "identification, characterization and understanding of any factor, passive or active, associated with the space domain that could affect space operations and thereby impact the security, safety, economy or environment of our nation" [3].

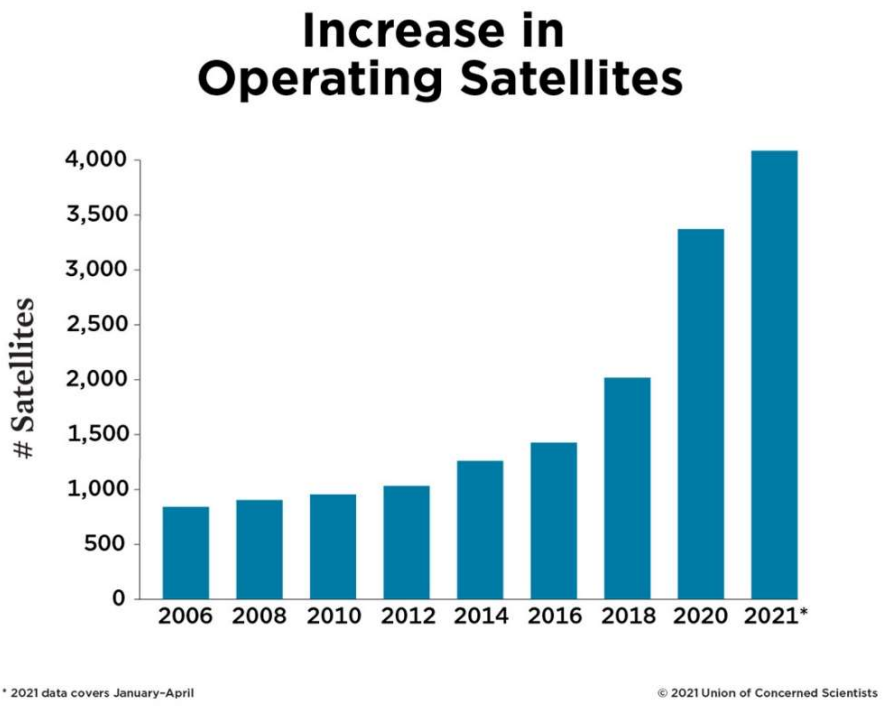

Figure 1: Graph taken from the Union of Concerned Scientists [4] **depicting the exponential growth of satellites orbiting the Earth.**

The 2021 *Annual Threat Assessment of The US Intelligence Community* cited both China and Russia as competitors to US dominance in the space domain as well as potential adversaries due to each country's development of counterspace weapons [5]. The United States Space Priorities Framework published in December 2021 states "The United States will defend its national security interests from the growing scope and scale of space and counterspace threats" [6]. In fact, on the 15th of November 2021, Russia tested an antisatellite (ASAT) missile against one of its defunct satellites [7]. Debris from this test forced the International Space Station (ISS) to make a maneuver. This maneuver was made just a week after the ISS had to make a separate maneuver to avoid debris which originated from a 2007 Chinese ASAT test [7].

According to NASA [8], there are over 27,000 pieces of orbital debris being tracked by the Department of Defense's Space Surveillance Network, with much more debris too small to be tracked. NASA considers millimeter-sized debris to represent the highest-mission ending risk to most robotic spacecraft in low-earth orbit with estimates totally 100 million pieces of millimeter-sized debris [8]. This issue is far from being solved or even mitigated, but fortunately in November 2021, the United States Space Force announced the Orbital Prime program. The goal of Orbital Prime is to incentivize companies to team up with academic or nonprofit organizations to compete in developing concepts for active debris removal [9].

To maintain function in the face of unpredictable threats, US space assets require agile support. Satellite constellations supporting mission-critical elements such as navigation or communication must be reconstituted quickly if the constellation is compromised either by attack or collision with debris or other satellites due to congestion. Additionally, congestion is a problem that will only continue to grow in scope as more satellites are launched to support activities on Earth and replace defunct satellites. In 2009 a defunct Russian spacecraft collided with a functioning Iridium satellite generating over 2,300 pieces of trackable debris [8]. It is only a matter of time before more collision like the Iridium collision happen due to over-congestion.

On-orbit-servicing (OOS) may help mitigate the issue of congestion by extending the operational lifetimes of satellites currently in orbit. By keeping satellites operational for longer, new satellites do not need to be launched into space and contribute to the problem. Northrop Grumman's Mission Extension Vehicle-1 (MEV-1) and Mission Extension Vehicle-2 (MEV-2) have paved the way for OOS by docking with, and

extending the operational life of, Intelsat 901 (IS-901) and Intelsat 10-02 (IS-10-02) respectively [10].

In 2019 it was demonstrated by A. Collins [11] that a cislunar-based refueling, repair, and replacement (R3) network may offer cost advantages over Earth-launched networks when servicing satellites in geosynchronous orbit (GEO). Cislunar orbits are also practically unused and offer a nearly risk-free environment for satellite storage as opposed to Earth orbits. Therefore, cislunar space offers an opportunity for agile response to the unpredictable risks faced by the US' space assets in GEO.

1.2 Problem Statement

This investigation attempts to answer two central research questions revolving around modeling an event-driven generalized multicommodity network flow (ED-GMCNF) to develop a dynamic optimal delivery scheduler to GEO from cislunar space:

1. Would a network using high-thrust or low-thrust delivery vehicles minimize the penalties associated with deviating from a required delivery schedule? Or would a combination of both vehicle types minimize deviation?
2. Within this network, will distant retrograde orbits (DROs) offer long-term fuel savings when compared to L_1 Lyapunov orbits as parking orbits for the delivery vehicles?

1.3 Thesis Overview

This investigation attempts to create an optimal delivery scheduler of both high-thrust and low-thrust R3 vehicles to GEO with a semi-major axis of 42,164 km. By developing

such a R3 network, the military can gain a significant advantage by ensuring the integrity of its critical satellite networks, the operational flexibility, and extending the operational lifetimes of the satellites within these networks. This thesis presents the investigation as follows:

- Chapter 1 introduces the problem and the motivation for investigation.
- Chapter 2 covers the mathematical and conceptual background of the investigation. A review of relevant literature is covered in this section as well.
- Chapter 3 describes the methodology of the investigation. In this section it is explained why the methodology of the investigation had to be shifted after the initial results and the updated methodology and research questions are presented.
- Chapter 4 presents and analyzes the results of the investigation.
- Chapter 5 summarizes the conclusions resulting from the investigation and provides suggestions for future works.

II. Background

Chapter Overview

This chapter presents a technical background to act as a primer to the main elements of this investigation. The primary objective of this thesis is to improve upon previous works to develop a cislunar logistics network which optimizes between fuel usage and time of flight for transfers. This necessitates investigations into several topics including: The circular restricted three-body problem (CR3BP), cislunar orbits, high thrust and low thrust cislunar trajectories, graph theory, generalized multicommodity network flows (GMCNFs), scheduling theory, and a brief overview of Hohmann transfers and inclination changes. These topics will be outlined in the following sections. Within each section the relevant mathematical basis will be presented along with the relevant history of each topic. Additionally, a brief overview of cislunar logistics and relevant literature will be presented. This section will conclude with a summary of the contributions to the literature that this investigation will provide.

2.1 The Circular Restricted Three-Body Problem

The CR3BP is a simplified case of the N-Body problem (NBP). The derivation of the equations of the CR3BP closely follows that of Collins' [11], who follows Wiesel's derivation [12]. The NBP is a system of N point masses whose gravitational forces are all mutually acting on a particle [11], [13]. According to Newton's second law of motion, the sum of the forces acting on a body is equal to its mass multiplied by its acceleration (Eq. 1). In the case of the CR3BP, the gravitational forces are the only forces acting on the particle. Eq. 2 gives Newton's Law of Gravitational motion where m_1 and m_2 are the

masses of the two bodies, G is the universal gravitational constant, and r is the distance between the two bodies. Eq. 1 can be combined with Newton's law of universal gravitation (Eq. 2) to produce Eq. 3 which is the equation of motion for body i in the NBP where the acceleration is given as $\ddot{\vec{r}}_i$ [11].

$$\sum \vec{F} = m\vec{a} \tag{1}$$

$$F = G\frac{m_1 m_2}{\left|\overrightarrow{r^2}\right|} \tag{2}$$

$$m_i \ddot{\vec{r}}_i = \sum_{j=1, j\neq i}^{N} G\frac{m_i m_j\left(\vec{r}_j - \vec{r}_i\right)}{\left|\vec{r}_j - \vec{r}_i\right|^3} \tag{3}$$

In the CR3BP, there are two primary bodies and a third body of comparatively negligible mass. The two primaries rotate about their barycenter in circular orbits and the third body is influenced by the gravity of the two primaries. Fig. 2 shows the synodic frame which is rotating with respect to the inertial frame at rate $\bar{\omega}$. In the synodic frame the Earth and the Moon are considered to be stationary and only the satellite appears to move. This problem is greatly simplified by defining nondimensional units from the properties of the two primary masses. The nondimensional mass parameter is defined by Eq. 4, which is then used to redefine the masses in Eq. 5a and 5b.

$$\mu = \frac{m_2}{m_1 + m_2} \tag{4}$$

$$m_1 = 1 - \mu \tag{5a}$$

$$m_2 = \mu \tag{5b}$$

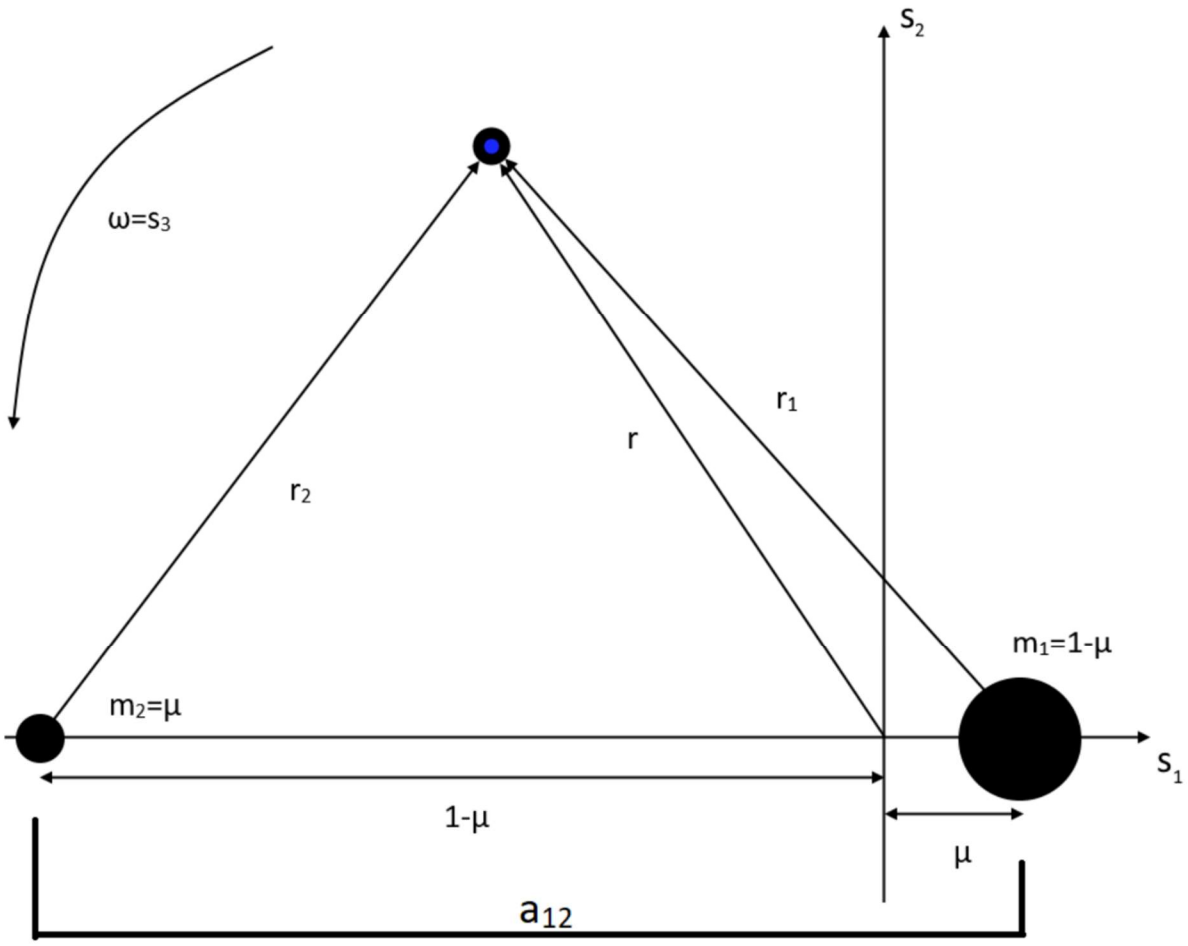

Figure 2: CR3BP Synodic Rotating Coordinate frame centered on the system's Barycenter. [Image credit: Collins [1], Wiesel [2]]

The characteristic length unit is defined as the scalar distance between the centers of mass of the two primary bodies a_{12} [11], [12]. The coordinates of the primary masses can then be defined as $x_1 = -\mu$ and $x_2 = 1 - \mu$. The nondimensional relative distance of the third body is given by Eq. 6, where the distances *x, y,* and *z* are divided by the characteristic length. By setting the characteristic time unit as the time it takes the

primary bodies to orbit around each other, Kepler's 3rd Law (Eq. 7) can be used to set the gravitational constant, *G*, equal to 1 in nondimensional units [11][12].

$$r_i = \sqrt{(x - x_i)^2 + y^2 + z^2} \tag{6}$$

$$T_{12} = 2\pi \sqrt{\frac{a_{12}^3}{G(m_1 + m_2)}} = 2\pi \tag{7}$$

The acceleration due to gravity on the third body—which will be a spacecraft in this investigation—can be seen in Eq. 8, which is the vector equation of motion. From this equation, the scalar equations of motion for the third body—in the rotating synodic frame—can be gathered (Eq. 9-11). From the scalar equations of motion, the locations of the Lagrange points of the system can be found by setting $\dot{x}, \dot{y}, \dot{z}, \ddot{x}, \ddot{y},$ and $\ddot{z}$ all equal to zero. After setting *y* and *z* to zero (Eq. 13,14), *x* can be solved for (Eq. 12) by the Newton-Raphson method, revealing the collinear Lagrange points [11], [12].

$$\ddot{\vec{r}} = \frac{(1-\mu)\,\vec{r_1}}{r_1^3} - \frac{\mu\,\vec{r_2}}{r_2^3} \tag{8}$$

$$\ddot{x} - 2\dot{y} - x = -\frac{(1-\mu)\,(x-\mu)}{r_1^3} - \frac{\mu\,(x+1-\mu)}{r_2^3} \tag{9}$$

$$\ddot{y} - 2\dot{x} - y = -\frac{(1-\mu)y}{r_1^3} - \frac{\mu y}{r_2^3} \tag{10}$$

$$\ddot{z} = -\frac{(1-\mu)z}{r_1^3} - \frac{\mu z}{r_2^3} \tag{11}$$

$$-x = -\frac{(1-\mu)\,(x-\mu)}{r_1^3} - \frac{\mu\,(x+1-\mu)}{r_2^3} \tag{12}$$

$$-y = -\frac{(1-\mu)y}{r_1^3} - \frac{\mu y}{r_2^3} \tag{13}$$

$$0 = -\frac{(1-\mu)z}{r_1^3} - \frac{\mu z}{r_2^3} \tag{14}$$

Any trajectories in the CR3BP must be calculated by numerical integration since there is no closed-form solution to the differential equations of the CR3BP. This is because the differential equations defining the CR3BP are highly coupled and nonlinear [14].

2.1.1 Lagrange Points

The Lagrange points are points of equilibrium within the CR3BP. At these points the gravitational and rotational forces reach a balance and a particle could theoretically stay at these points indefinitely. The L_1, L_2, and L_3 Lagrange points (collinear points) are unstable, meaning that small perturbations to repeating trajectories around these points can lead to large differences in future positions. The L_4 and L_5 Lagrange points (triangular points) are considered stable; however, due to perturbations, objects are not likely to stay in these positions. The Lagrange points can be seen depicted in Fig. 3.

In Eq. 11, it can be seen that when $\ddot{z}$ is equal to zero, z must also be zero, leading to Eq. 14. This indicates that the Lagrange points are all within the plane of the primaries. The collinear Lagrange points were the first three Lagrange points discovered in 1765 by Leonhard Euler [15]. The other two Lagrange points—the so-called equilateral triangular points—were discovered by Lagrange in 1772.

While the equilateral triangle points can be solved simply by geometry, deriving these points using the pseudopotential helps to build a greater understanding.

The potential function is defined as:

$$U(x,y,z) = \frac{1}{2}(x^2 + y^2) + \frac{1-\mu}{r_1} + \frac{\mu}{r_2} \tag{15}$$

and Eqs. 9, 10, and 11 can be rewritten as the partial derivatives of the potential function:

$$\ddot{x} - 2\dot{y} = x - \frac{(1-\mu)\,(x-\mu)}{r_1^3} - \frac{\mu\,(x+1-\mu)}{r_2^3} = \frac{\partial U}{\partial x} = U_x \tag{16}$$

$$\ddot{y} - 2\dot{x} = y\left(1 - \frac{(1-\mu)}{r_1^3} - \frac{\mu}{r_2^3}\right) = \frac{\partial U}{\partial y} = U_y \tag{17}$$

$$\ddot{z} = -\frac{(1-\mu)z}{r_1^3} - \frac{\mu z}{r_2^3} == \frac{\partial U}{\partial z} = U_z \tag{18}$$

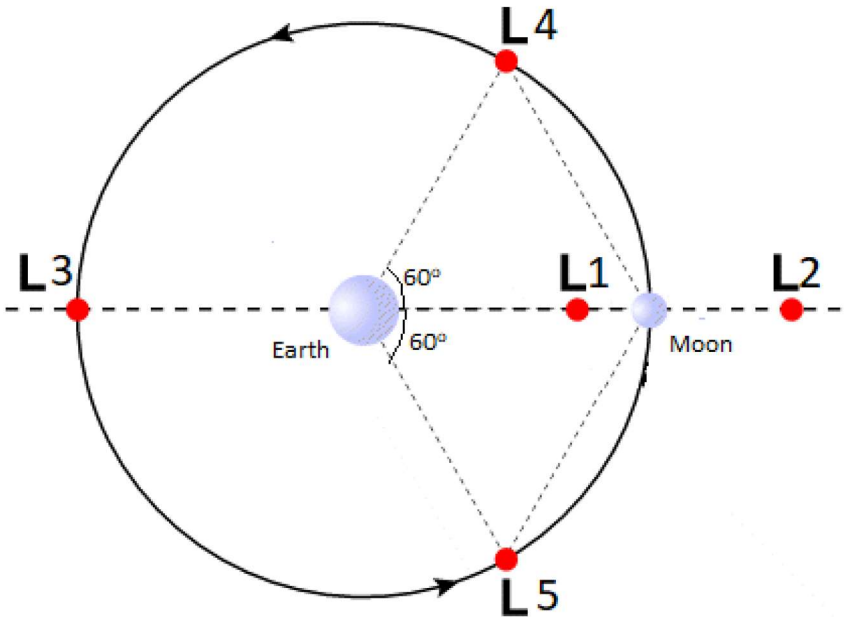

Figure 3: The Five Earth-Moon Lagrange Points. L_1, L_2, and L_3 are commonly referred to as the collinear Lagrange points with L_4 and L_5 commonly referred to as the equilateral triangular points. (Graphic from Collins [1])

The triangular points still lie in the same plane as the primaries ($z = 0$) but are not collinear ($y \neq 0$). The partial derivatives of the pseudopotential with respect to x and y must be zero at a Lagrange point. At an equilateral point, $y \neq 0$, so Eq. 19 must be satisfied:

$$1 - \frac{(1-\mu)}{r_1^3} - \frac{\mu}{r_2^3} = 0 \tag{19}$$

Expanding Eq. 16 yields:

$$x - \frac{(1-\mu)\,(x-\mu)}{r_1^3} - \frac{\mu\,(x+1-\mu)}{r_2^3} = x - \frac{x - x\mu + \mu - \mu^2}{r_1^3} - \frac{x\mu - \mu + \mu^2}{r_2^3} = 0 \tag{20}$$

Which can be rearranged to show:

$$\frac{\mu - \mu^2}{r_1^3} + \frac{\mu^2 - \mu}{r_2^3} = x\left(1 - \frac{(1-\mu)}{r_1^3} - \frac{\mu}{r_2^3}\right) \tag{21}$$

Finally, after substituting Eq. 19 and rearranging:

$$\frac{\mu - \mu^2}{r_1^3} = \frac{\mu - \mu^2}{r_2^3} \tag{22}$$

From Eqs. 12, 13, and 22 it can be seen that the equilateral points result when $r_1 = r_2 = 1$. This implies an x-location of $x = \frac{1}{2} - \mu$ for L_4 and L_5 and y-locations at $y = \pm\frac{\sqrt{3}}{2}$. Note that the distances between the Earth, Moon, and the L4 and L5 Lagrange points form two equilateral triangles. The Lagrange points each serve as a vertex and the Earth and Moon serving as the other vertices.

The Lagrange points are an important area of focus to both military, scientific, and commercial applications. Satellites can be put in orbits about Lagrange points that require minimal station keeping. These satellites can have a host of uses from Space

Domain Awareness (SDA) and communications, to potentially parking R3 satellites. Ostman [13] investigated using transfers through the Sun-exclusion zone to the L_1 and L_2 Lagrange points, offering the potential to protect satellites from tracking, at the expense of significant fuel cost. Collins [11] investigated using the L_1 and L_2 points as nodes within the development of a cislunar logistics network for R3. This investigation found that using cislunar parking orbits for R3 missions may present an advantage when accounting for Lunar in-situ resource utilization (ISRU), but otherwise would likely be infeasible.

2.2 Cislunar Orbits

Cislunar space is widely accepted as the space extending beyond GEO and into the regime of the Moon. This is a volume of space stretching from a single multiple of GEO out to thirteen times the radius of GEO [16]. Within the radius of GEO, the effects of Earth's gravity are dominant, and the gravitational effects of the Moon can be largely ignored. However, in cislunar space the gravitational effects of the Moon increase, eventually becoming large enough to balance the Earth's gravity; this leads to the Lagrange points.

A number of different periodic orbits about the Lagrange points have been considered for cislunar architectures within the literature. Figs. 4 and 5 gives examples of some of the types of cislunar orbits. Zimovan-Spreen et al. [17] investigated near rectilinear halo orbits (NRHOs) around the L1 and L2 Lagrange points and found the possibility of eclipse avoidance. Avoiding eclipse allows the spacecraft in this orbit to remain in constant view with the Earth, which would be necessary for manned space-

stations placed in these orbits. Jagannatha [18] investigates the use of halo orbits around L1 and L2 as way stations for refueling and resupplying crewed deep-space missions. Cislunar orbits also offer an advantage for low-cost inclination changes as Collins [11] indicates which may be of use to transferring vehicles since inclination changes near primary bodies are ΔV-intensive.

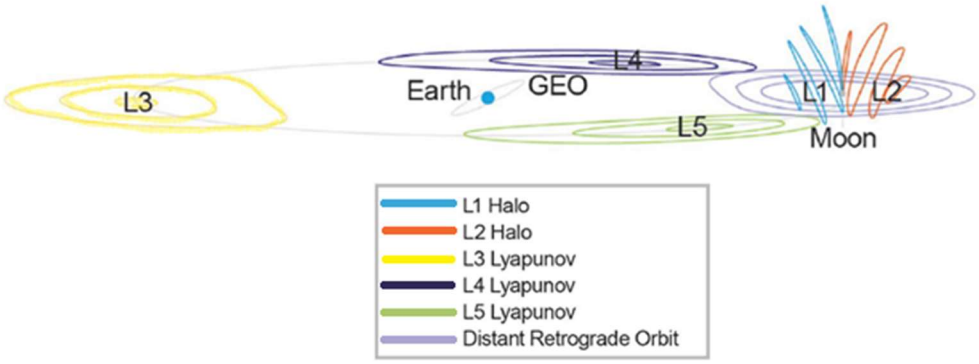

Figure 4: The types of periodic orbits in the Earth-Moon CR3BP. Note GEO is included for scale. Edited in Paint. Taken from [16], provided originally by the Aerospace Corporation.

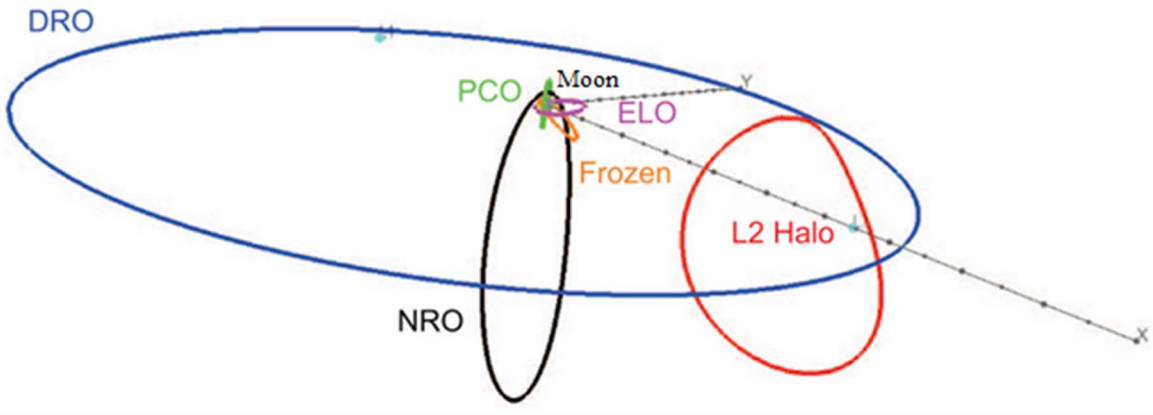

Figure 5: Types of periodic orbits including a Near Rectilinear Orbit (NRO), L_2 Halo, Distant Retrograde Orbit (DRO), Prograde Circular Orbit (PCO), Eliptical Lunar Orbit (ELO), and a frozen orbit. Note that the NRO orbit can be flipped to pass closer to the south Lunar pole. Figure taken from Whitley [19], edited in paint.

2.2.1 Lyapunov Orbits

A Lyapunov orbit is a planar periodic orbit in the CR3BP that orbits about a collinear Lagrange point [20]. These orbits have been studied extensively for establishing cislunar architectures. Ostman's investigation [13] used families of Lyapunov orbits around the L_1 and L_2 points. Collins [11] considers the Lyapunov orbits about the L_1 and L_2 points to develop a cislunar logistics network for R3. Knister's investigation [21] of cislunar SDA and Space Traffic Management (STM) used a reference architecture of a single satellite in a L_1 Lyapunov orbit.

Lyapunov orbits take advantage of planar, periodic, symmetric motion about the collinear Lagrange points. Lyapunov orbits are restricted to the x-y plane. Thus, to develop a Lyapunov orbit, it is assumed the initial state vector lies on the x-axis with

parameters calculated from the first-order linearized approximation of the equations of motion [22]. These equations of motion can be written in simplified form as:

$$\xi = -A_\xi \cos(s\tau + \phi) \tag{23}$$

$$\eta = \beta_3 A_\xi \sin(s\tau + \phi) \tag{24}$$

Where ξ is the x-component of motion about the Lagrange point, η is the y-component of motion about the Lagrange point, A_ξ is the orbital amplitude in the x-direction, and β_3 is a function of the orbit frequency *s*:

$$s = \sqrt{\beta_1 + (\beta_1^2 + \beta_2^2)^{\frac{1}{2}}} \tag{25}$$

$$\beta_1 = 2 - \frac{U_{xx} + U_{yy}}{2} \tag{26}$$

$$\beta_2^2 = -U_{xx}U_{yy} > 0 \tag{27}$$

$$\beta_3 = \frac{s^2 - U_{xx}}{2s} \tag{28}$$

And U_{xx}, U_{yy} are the second partial derivatives of the pseudopotential:

$$U_{xx} = 1 - \frac{1-\mu}{\rho_1^3} + \frac{3\big((x+\mu)^2(1-\mu)\big)}{\rho_1^5} - \frac{\mu}{\rho_2^3} + \frac{3\Big(\big(x-(1-\mu)\big)^2\mu\Big)}{\rho_2^5} \tag{29}$$

$$U_{yy} = 1 - \frac{1-\mu}{\rho_1^3} + \frac{3y^2(1-\mu)}{\rho_1^5} - \frac{\mu}{\rho_2^3} + \frac{3y^2\mu}{\rho_2^5} \tag{30}$$

The state vector defined by these parameters is:

$$\boldsymbol{X}_0 = \begin{bmatrix} x_0 \\ 0 \\ 0 \\ \dot{y}_0 \\ 0 \\ 0 \end{bmatrix} \tag{31}$$

Symmetry occurs once the initial conditions are modified such that the first crossing of the x-z plane yields a $-\dot{y}_0$ velocity in the y-direction for half of a period [21]. This can be done by propagating iterations of the trajectory using the State Transition Matrix, assessing the error between the end state and the desired state, and varying the control parameters until the y-direction velocity error is below the chosen threshold [21]. This can be achieved through a differential corrections technique such as the simple shooting method, as used by Ostman [13], [21].

2.2.2 Halo Orbits

Halo orbits—in the context of the Earth-Moon CR3BP—are the family of periodic orbits around the L_1 and L_2 Lagrange points which pass through the orbital plane of the Moon [16]. Halo orbits are of great interest due to their characteristics of continuous visibility and ease of accessibility from Earth [19]. Halo orbits appear to orbit around the Moon and are always visible from the Earth's perspective. Whitley [19] evaluated Earth-accessibility of various staging orbits using ΔV requirements for the Orion spacecraft and found halo orbits to be favorable at 637 m/s for an optimized 31-day mission. Halo orbits are also purely periodic in the CR3BP and semi-stable, making them desirable for their predictable behavior and low maintenance costs [19]. For these reasons, halo orbits are being considered for a number of different missions. In Whitley's [19] investigation of cislunar staging orbits, it is noted that NASA's upcoming Artemis mission will require less than five meters per second of ΔV per year for station-keeping for a halo orbit about the L_2 Lagrange point.

The formation of halo orbits around L_1 and L_2 were examined in the analysis by Chongrui [23]. Two strategies were proposed for maintaining the halo orbits. The first

method proposes using a small impulse at each half cycle of the orbit to ensure the spacecraft crosses the orbital plane with a perpendicular velocity. The second method proposes using the periodicity of perturbations to the orbit to create a multi-circular halo orbit in resonance with the perturbations. This method requires additional corrections to the orbit. Recent missions CHANG'E 2 and Queqiao of the Chinese National Space Administration demonstrate the feasibility of the first method [23].

2.2.3 Near Rectilinear Halo Orbits (NRHOs)

A variation of the halo orbit family are the NRHOs. These orbits are characterized by a close approach to one of the Lunar poles at periapsis and a significantly more distant apoapsis of up to 75,000 km from the opposite pole [24]. The NRHOs have the benefit of providing access to the surfaces of the Lunar poles. Like regular halo orbits, NRHOs require minimal station-keeping ΔV due to the only slightly unstable periodic nature of the orbit and also provide continuous Earth-visibility [19], [24]. The distant apoapsis of the NRHOs also offer the added advantage of low-cost inclination changes since these maneuvers are more efficient when done at a lower velocity further from the orbiting body [24].

In Lantoine's [24] investigation, a methodology for determining efficient transfers from NRHOs to distant retrograde orbits (DROs) was established. Lantoine [24] noted these orbits are attractive for future missions including manned and unmanned surface missions as well as NASA's proposed Asteroid Redirected Robotic Mission.

Whitley [25] examined and compared NRHOs to bifurcated butterfly orbits about the L_2 point in the context of upcoming crewed and uncrewed NASA missions. While butterfly orbits will not be considered in this investigation, it is noteworthy that Whitley

[25] found that butterfly orbits that bifurcate from the NHROs reduce the costs of landing at either the Lunar equator or Lunar Poles. Butterfly orbits appear to be attractive cislunar staging orbits [25].

2.2.4 Distant Retrograde Orbits (DROs)

DROs are a family of periodic orbits about the secondary body (e.g. the Moon) in the retrograde direction within the CR3BP [19],[22]. DROs lie within the orbital plane of the Moon and have an elliptical orbit symmetrical about the x-axis in the rotating frame [24]. As covered by Lantoine [24], DROs are also only slightly unstable and thusly are desirable as a cislunar parking orbit as station-keeping requirements would be at a minimum. Lantoine [24] found optimal transfers from a family of NRHOs with a 9:2 resonance[1] to a family of DROs with a minimum distance of 70,000 km from the Lunar surface.

In 2014 Capdevila [26] investigated using impulsive maneuvers to transfer from LEO to various DROs and compared the different station-keeping cost of DROs and other orbits. Notably, Capdevila [26] found that DROs require lower station-keeping costs that increase more slowly than the L_1 Lyapunov orbits considered. In 2018 Capdevila [27] explored the possibility of using DROs and NRHOs as staging orbits due to the stable nature of these orbits. Similar to Capdevila's 2014 investigation, Bezrouk [28] investigated DROs citing NASA's Asteroid Redirect Mission (ARM) as motivation. In contrast, Bezrouk [28] examined the stability of DROs at various orbit sizes to

[1] Resonance refers to the ratio of orbits between the orbiting body (i.e. the satellite) and the orbits of the primary body (the Moon in this case). The 9:2 resonance refers to nine orbits of the satellite around the Moon for every two orbits of the Moon around the Earth. Resonance therefore defines the size of a DRO, for example a 4:2 resonance will have a smaller orbit around the Moon than a 9:2 resonance since the satellite orbits four times every time the Moon orbits the Earth twice as opposed to orbiting nine times in the same timeframe.

determine which orbits were most resistant to perturbations in the context of capturing, towing, and storing an asteroid in the most stable orbit as part of ARM. Bezrouk [28] concluded that DROs between 60,000 and 68,000 km in x-amplitude in the synodic reference frame are most stable and therefore most suitable for a mission such as ARM.

2.2.5 Distant Prograde Orbits (DPOs)

The DPO is a family of periodic orbits which orbit about the secondary body in the prograde direction within the CR3BP [22]. DPOs are unstable and symmetric about the x-axis when they are simple periodic, as can be seen in Fig. 6. The period of a DPO is generally on the order of 2-4 weeks [22]. DPOs offer attractive characteristics for cislunar mission design. In the realm of communications, a DPO can offer constant contact with the far side of the moon with only one spacecraft [29]. Unlike the Lagrange point orbits, DPOs can offer close flybys with the Moon which may offer an advantage for payload delivery, or for the case of this investigation, launch from the Moon [29]. Another attractive characteristic of the DPO is that within the CR3BP, it has the same Jacobi constant as unstable orbits about L_1 and L_2. This fact allows for a free transfer—i.e. a transfer requiring no ΔV—between the two families of orbits and is desirable for a number of potential mission designs [22].

Low-energy transfers to DPOs are a frequent topic in the literature. Parker and Anderson [22] cover the topic of low-energy transfers between periodic orbits as well as between the Earth and the Moon extensively. Mingotti [29], presents an impulsive-thrust method as well as a continuous-thrust method for transferring a spacecraft to DPOs around the Moon. This work [29] exploits the invariant manifolds of the DPOs such that the impulsive trajectories target the stable manifold from the exterior and the continuous-

thrust trajectories target the stable manifold from the interior, as also described by Parker and Anderson [22]. Mingotti [29] found no significant cost savings between high-thrust and low-thrust transfers to DPO, but low-thrust transfers required a second maneuver to stabilize the spacecraft around the Moon whereas the high-thrust transfer did not. This finding may be important for future mission scenarios similar to the one in this investigation considering the cost-savings in a network of high and low thrust trajectories between the Earth and the Moon.

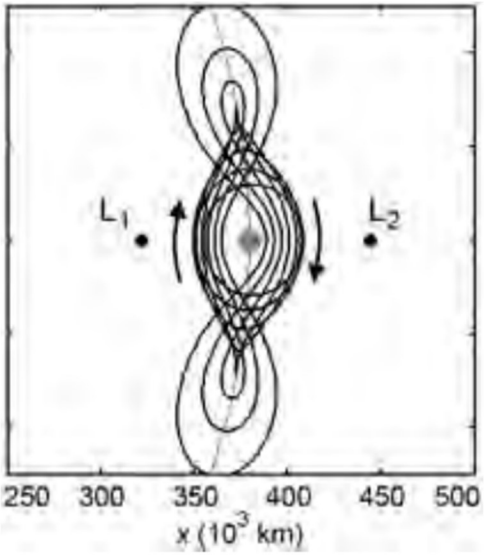

Figure 6: Example of a family of DPOs about the Moon. Taken from Parker and Anderson [22]**.**

2.3 Cislunar Trajectories

Within the context of this investigation, only trajectories from geosynchronous orbit (GEO) at 42,164 km in altitude from the Earth to cislunar space will be considered and vice versa. However, more broadly a cislunar trajectory refers to a trajectory between the Earth's sphere of influence and the Moon's sphere of influence in space. Perhaps the

most famous examples of cislunar trajectories are the trajectories used by the Apollo missions. Cislunar trajectories have been investigated extensively within the literature and can be broken up into two categories: impulsive, high-thrust trajectories and continuous, low-thrust trajectories.

Both impulsive and continuous thrust trajectories can leverage invariant manifolds for low-energy trajectories to cislunar space [29]. The invariant manifolds are the sets of trajectories a spacecraft follows in the CR3BP when it is perturbed from some initial position on a periodic orbit solution [22]. The unstable invariant manifold is the set of trajectories exponentially leading away from an unstable periodic orbit that a spacecraft will follow if perturbed from the orbit in the unstable direction as defined by the eigenvectors of Jacobian of each state along the orbit. The stable invariant manifold is set of trajectories a spacecraft will take to asymptotically approach the unstable periodic orbit along that orbit's stable eigenvector [22].

2.3.1 High-Thrust Trajectories

High-thrust trajectories are generally considered to be impulsive because the burn duration is much shorter than the coasting duration. A burn may last on the order of tens of seconds whereas the coasting portion of the maneuver will generally last many hours. Spacecraft which rely on chemical propulsion are generally considered to be high-thrust. Impulsive trajectories generally only have a handful of burns. The first burn is needed to exit the current orbit and enter the transfer trajectory. The next burn is needed to exit the transfer trajectory and insert into the new orbit. Corrective maneuvers are used as needed in-between the two orbits to maintain the transfer trajectory.

In the investigation by Butcher [30], a guidance scheme is developed using impulsive maneuvers to inject into and stay on the stable manifold of a L_1 halo orbit. This is done because manifolds of the Lagrange points offer opportunities for low-cost transfers between Earth orbits and Lagrange point orbits like those discussed in Section 2.2. The guidance scheme developed by Butcher [30] is able to compensate for errors during manifold injection and demonstrates that a single-burn scheme is more effective than a two-burn scheme due to the reduction in impulsive maneuvers resulting in less thrust errors. Fig. 7 depicts a high-thrust trajectory taken from the investigation of continuous thrust vs. impulsive thrust Earth-Moon transfers by Lee et al. [31], discussed in section 2.3.2.

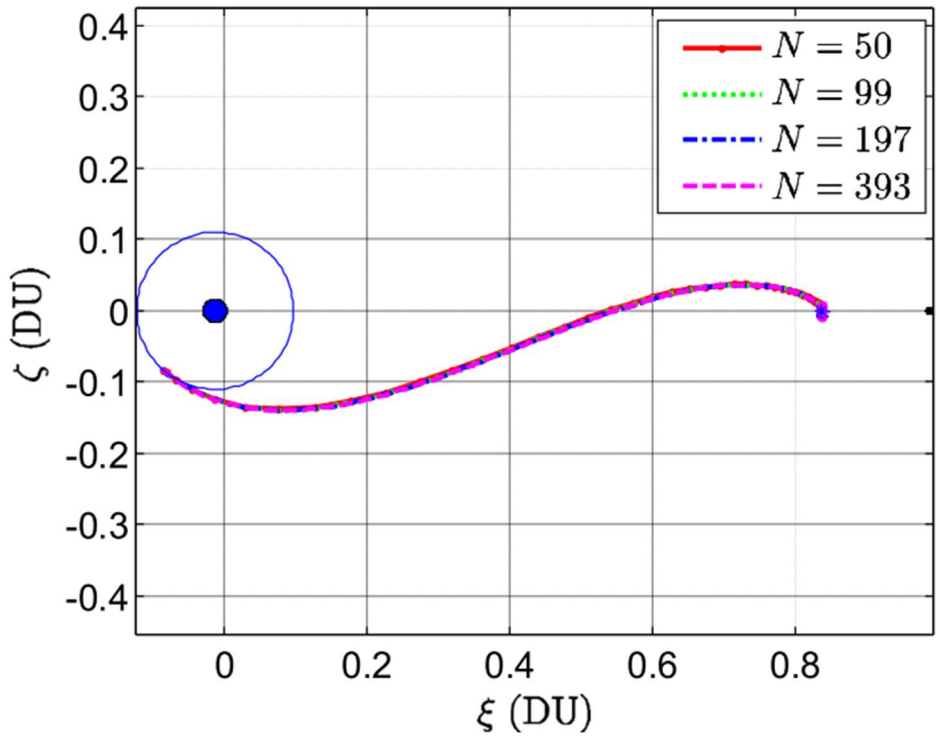

Figure 7: Example high-thrust, impulsive trajectory from Earth to L_1. Taken from [31].

2.3.2 Low-Thrust Trajectories

Spacecraft with low-thrust propulsion systems typically use electric propulsion to produce continuous—or near continuous—thrust for long durations. Electric propulsion is often considered desirable because of the very high specific impulse allowed by electric propulsion engines. The propellant also does not need an ignition source which adds further desirability. These systems typically rely on ionizing a noble gas and accelerating it through an electric field, out of the exhaust nozzle at a high velocity [32]. The exhaust velocity of electric propulsion is typically an order of magnitude greater than that of chemical propulsion systems; however, the mass of the exhaust is significantly less which ultimately causes the thrust to be much lower than a high-thrust system [32].

Parrish [32] develops an optimization method for low-thrust trajectories within cislunar and translunar space. The method developed relies on the use of neural networks to correct low-thrust reference trajectories and tested transfers from DROs-to-NRHOs, DROs-to-DROs, and L_2 Halo-to-L_2 Halo. Parrish [32] demonstrates that neural networks can improve the speed and robustness of solving trajectory optimization problems within the Earth-Moon system. Maodeng [33] uses a combination of numerical and analytical methods to generate families of Lyapunov orbits around L_1 and locate the stable and unstable manifolds of these orbits to be used for low-thrust trajectories. A genetic algorithm is then used to optimize the trajectories. The optimization results in a solution which saves 221 m/s of ΔV when compared to a Hohmann transfer at the expense of a greater TOF [33].

Lee et al. [31] compared the optimality of impulsive-thrust transfer trajectories from GEO to an L_1 Lyapunov orbit versus continuous-thrust transfer trajectories using

either a minimum fuel performance index or a quadratic performance index. A direct departure transfer method was used for the impulsive-thrust transfers and a spiral departure trajectory for the continuous thrust transfers. Both transfer methods were constrained to a TOF of 6 days. Lee et al. [31] found that when using a minimum fuel performance index, the direct departure transfer resulted in a savings of 167 m/s ΔV.

Qu et al. [34] optimize low-thrust trajectories using a gradient-based design methodology. The trajectories explored are Earth-Moon trajectories which enter an L_1 halo orbit from the invariant manifold. A low-thrust trajectory targeting L_1 from this investigation is displayed in Fig. 8 as an example.

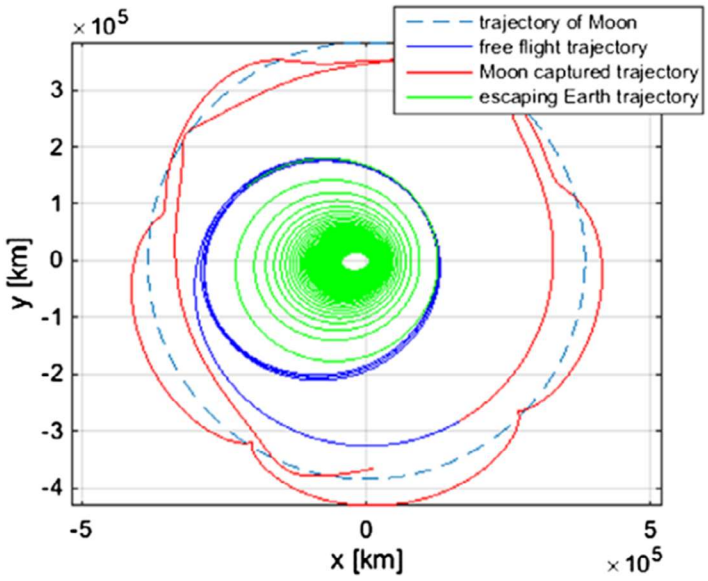

Figure 8: Example of a low-thrust trajectory. Note the spiraling of the trajectory as the satellite gradually raises its orbit. Taken from [34].

2.4 Graph Theory

A graph-theoretic approach is often used in modeling logistics networks. This means building a graph—i.e. network—of nodes which are connected by arcs [35]–[37].

The network is represented as a graph $G(V, E)$ of vertices and edges. Arcs and nodes can be used interchangeably with edges and vertices. Edges connect vertices and are associated with some positive integer defining the capacity of the edge. The capacity limits how much of a commodity can travel along that edge. A positive integer associated with a vertex is the conservation condition of that vertex. This condition defines the amount of commodity which flows into the vertex and must also subsequently flow out of the vertex. The source vertex defines where the flow of the network begins. The sink vertex defines the end position of the flow. The goal of the graph is to maximize the flow across the network from the source to the sink per unit of time [36], [37].

In unidirectional network flows commodities are only allowed movement in one direction. However, in this investigation, a bi-directed network flow will be assumed. In bi-directed network flows commodities are not required to only move "forward" in the graph from the source to the sink. In these problems, each arc may have a capacity to it limiting the amount of commodity that can move along that arc. Additionally, each arc may have a cost associated with moving a commodity across it. Similarly, nodes may also have capacities and costs associated with them [35]–[37].

The goal of a classic network flow problem is to meet the demand across the network by maximizing flow and minimizing costs. Each node may need a certain amount of commodity to satisfy demand. As a simplified, terrestrial example, a business such as Amazon solves network flow problems daily. Amazon may need to meet demand for one of their products in a warehouse in Seattle—this would be the sink node—and a warehouse in Portland has excess of that product —Portland would be the source node. The problem becomes minimizing the cost of shipping the necessary amount of the

product to meet the demand. In the case of the multicommodity flow, Amazon would be looking to meet the demand of more than one product at the warehouse in Seattle. Amazon is an Earth-based logistics system used to introduce the idea of a logistics network. This investigation will be taking the same idea of such a logistics network and applying it to cislunar space.

Fig. 9 depicts a simple network flow model. In this hypothetical example, the arc from the source to node *A* has a cost of four associated with it. In real terms this cost could be the cost of fuel, wear and tear on a vehicle, or some other metric. The path that minimizes cost from the source to the sink would be to use the arc connecting the source and node *B* and then the arc connecting node *B* to node *A*. From node *A* the arc to the sink would then be taken to complete the flow with minimal cost. However, if there is a capacity constraint on one of the arcs, this may not maximize flow and another path may be optimal.

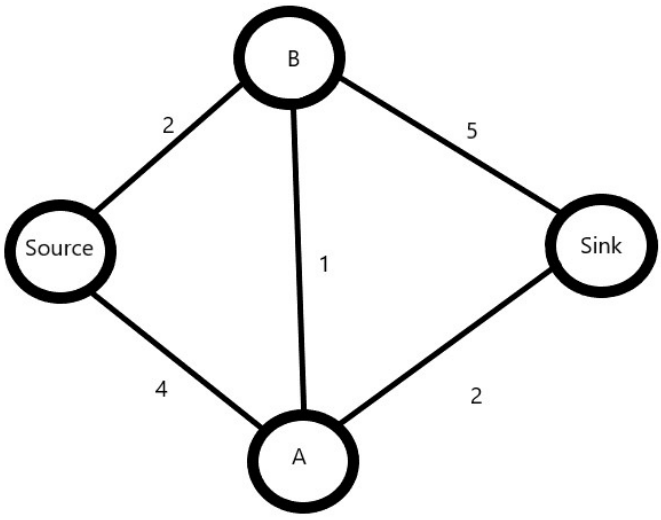

Figure 9: An example network demonstrating the cost to flow across a network with arc costs.

2.5 Generalized Multicommodity Network Flows (GMCNFs)

The GMCNF is often used when developing space logistics networks [11], [18], [35], [38], [39]. Collins' investigation [11] used a modified version of the GMCNF. Ishimatsu [35] developed a GMCNF to model space logistics networks for human exploration of Mars. Ishimatsu [38] later developed a GMCNF model for an Earth-Moon-Mars Logistics system and determined Lunar ISRU became desirable at productivity levels greater than 1.8 kg of fuel per year per kg mass launched from Earth. Jagannatha [18] developed a novel GMCNF modification to better include low-thrust spacecraft in an attempt to maximize the tradeoffs between cost, fuel, and technology.

A GMCNF is a special case of the classic network flow problem in which the flow across arcs may not be conserved [35]. In the classical network flow, it is assumed that the quantity of the commodity traveling across the arc stays the same. However, there are cases where this idealization is violated in real life and the commodity is consumed—i.e. not conserved—in the process of traveling across the arc. As Ishimatsu [35] describes, an example of this is the loss of power over a distance during transmission of electrical power through the power grid.

The mathematical formulation of the GMCNF will follow the form of Ishimatsu [35]. Let x_{ij}^{k} denote the amount of commodity k traveling from node i to node j. μ_{ij} is a positive multiplier $0 < \mu_{ij} < 1$ that represents the consumption of commodity k when traveling from node i to node j. The cost associated with traveling along the arc from node i to node j is c_ij. The GMCNF problem is presented as follows:

Minimize:

$$J = \sum_{(i,j)\in A} c_{ij} x_{ij} \tag{15}$$

Subject to:

$$\sum_{(i,j)\in A} x_{ij} - \sum_{(i,j)\in A} \mu_{ji} x_{ji} \leq b_i \; \forall \; i \in N \tag{16}$$

$$\forall \; (i,j) \in A \tag{17}$$

Where (i,j) is the arc from node i to node j. A represents all of the arcs in the network and N is the number of nodes. b_i represents the demand at node i. If $b_i > 0$ node i is a supply node; if $b_i < 0$ node i is a demand node; and if $b_i = 0$ node i is a transshipment node. Eq. 16 represents the amount of commodity remaining after accounting for the amount of commodity consumed when traveling from i to j.

2.5.1 Event-Driven Generalized Multicommodity Network Flows (ED-GMCNFs)

Ho [40] improved upon the GMCNF by incorporating a time dimension to the static GMCNF. The dimension of time was incorporated by essentially stacking layers of GMCNFs and creating a 3D structure of nodes [11]. This formulation is known as the Time-Expanded GMCNF (TE-GMCNF). Within the TE-GMCNF arcs represent a discrete movement through time. However, as brought up by Jaganatha in developing the Event-Driven GMCNF[18], [39] when modeling space logistics networks, the TE-GMCNF cannot incorporate low-thrust trajectories.

These trajectories cannot be accounted for in the TE-GMCNF formulation because space vehicles moving commodities on low-thrust trajectories have a time-of-flight (TOF) highly dependent on the total mass of the vehicle [18], [39]. Therefore, the

arcs representing low-thrust trajectories would be flow dependent and could not be calculated beforehand to fit within the discrete time steps of the TE-GMCNF. Instead of duplicating the GMCNF at discrete time steps between event layers like the TE-GMCNF, the ED-GMCNF duplicates the GMCNF at variable-length time steps otherwise known as event steps [11], [18], [39]. Fig. 10 demonstrates the difference between the ED-GMCNF and the TE-GMCNF.

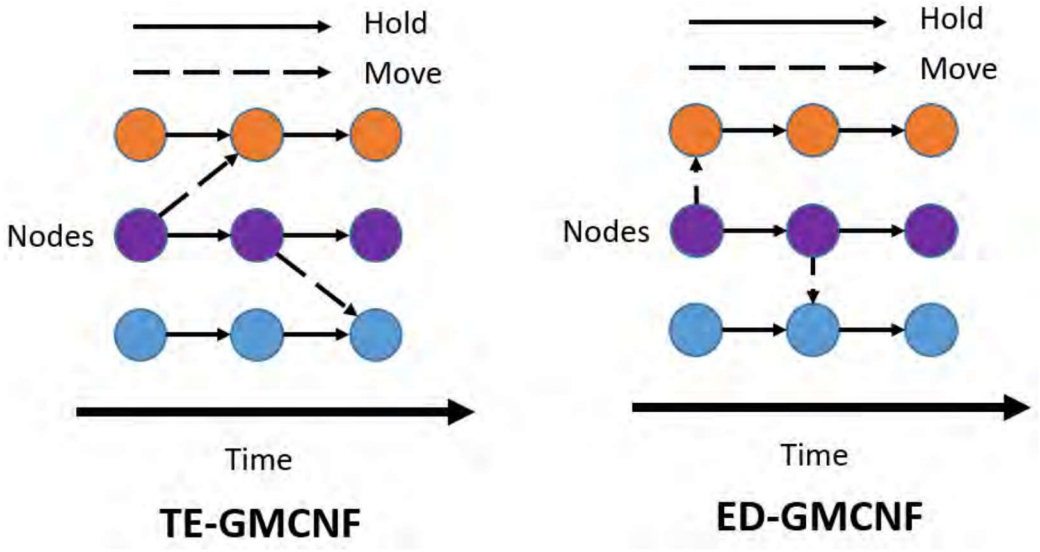

Figure 10: Examples of the TE-GMCNF and ED-GMCNF. Note that the movement arcs in the TE-GMCNF encompass the passage of time as well as the movement of a commodity, whereas the movement between space and time are separate in the ED-GMCNF. Figure taken from Collins [11].

2.6 Cislunar Logistics

With a growing human presence in space, logistics networks will be of ever-growing importance. R3 networks using cislunar orbits as staging orbits may be able to support satellites orbiting Earth and beyond. These networks may also be able to support

missions on the Moon and in cislunar space, especially with an increase in missions on the Lunar surface for ISRU. The investigation into using cislunar staging orbits by Capdevila [27] also proposes using the cislunar region as the central node of a space network within the Earth-Moon system. This is proposed due to the natural gravitational dynamics of the Earth-Moon system which manifest in different forms within the cislunar domain. Fig. 11 displays the concept of using cislunar space as a central node.

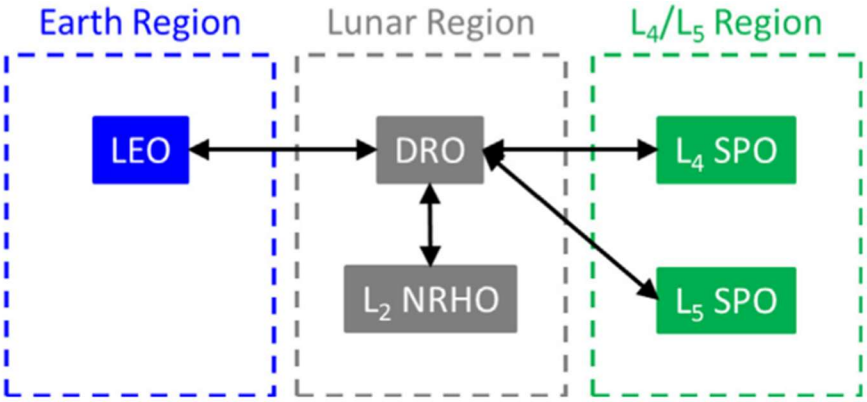

Figure 11: Superficial diagram of a potential network using the Lunar region as the central node linking the Earth region of space to different regions within the Earth-Moon system. Taken from Capdevila [27].

While beyond the scope of this investigation, cislunar SDA makes up a significant portion of the literature. Cislunar SDA will be necessary to support increased traffic between the Earth and the Moon which would further necessitate support from a cislunar-based R3 network. In the investigation by Nallapu [41], a design architecture for cislunar missions that focuses on selecting Lagrange point orbits based on optimal coverage, station-keeping, and optimal transfers is formulated. The three overarching themes set by the Lunar Exploration and Analysis Group:

- Study Lunar resources and the strategic knowledge gaps related to human exploration of the Lunar surface
- Study the effect of the Lunar environment on humans on the Lunar surface
- Enable working and living on the Moon

are cited and used as the motivation to form a cislunar communications architecture in the study. The "Integrated Design Engineering and Automation of Swarms" (IDEAS) architecture is used to find the optimal solution to the problems of trajectory design, spacecraft design, and swarm mission design. It was found that a constellation of three total spacecraft in a L_1 north halo orbit, a L_1 south halo orbit, and L_2 south halo orbit can maximize coverage of the Lunar surface and minimize the fuel constraints of orbit insertion and station-keeping [41].

Currently, the Moon is being considered for ISRU due to the availability of icy regolith. Thermal mining appears to be a viable method for extracting water from the Moon's regolith [42]. Thermal mining targets surface and near-subsurface ice within the regolith by redirecting sunlight. The redirected sunlight heats up the regolith causing the water-ice to sublimate so that the vapors can be captured. To turn the water into propellant, energy from sunlight is captured to power an electrolysis process and separate the water into hydrogen and oxygen. Sowers [42] found that lunar sourced propellant is an order of magnitude less expensive than propellant launched from Earth when used in high Earth orbits.

Once sourced, the propellant can be launched to numerous different cislunar orbits with close passes to the Lunar surface. As mentioned earlier, Whitley [25] found that butterfly orbits that bifurcate from the NHROs reduce the costs of landing at either

the Lunar equator or Lunar Poles—the poles being a prime location of ice deposits. It is also known that DPOs offer close flybys of the Lunar surface and low cost transfers between the unstable periodic orbits of the Lagrange points [22], [29].

Liquid oxygen and liquid hydrogen can be used as propellant for high-thrust propulsion systems, but not for continuous thrust which primarily depends on noble gasses. It is known that noble gasses exist on the Moon [43], but there does not appear to be much literature on extraction viability and technological availability for refueling continuous-thrust propulsion systems.

2.6.1 Cislunar Missions

Future cislunar missions will include various forms from tracking and categorizing space objects through SDA and STM to extending mission life with R3 and ISRU. As shown by Collins [11], creating a cislunar R3 network will likely only be feasible with ISRU. Barring any significant technology leaps, R3 missions originating from cislunar parking orbits will likely typically occur in GEO as opposed to LEO, following the results of Collins' simulation [11]. Cislunar space also offers challenges in SDA whose solution is garnering attention for various applications.

As noted in the primer on cislunar space by Holzinger [16], due to the vast volume and extreme distances contained within cislunar space, as well as the dynamics of the Earth-Moon system as it revolves around the Sun, no single detector—space-based or Earth-based—is fit for the job. SDA in cislunar space will require an entire network. An example of this is the cislunar Autonomous Positioning System Technology Operations and Navigation Experiment (CAPSTONE) funded by NASA [16], [44]. The goal of CAPSTONE is to demonstrate the feasibility of using NRHOs as staging orbits for

spacecraft to construct a Cislunar Autonomous Positioning System (CAPS) which will enable peer-to-peer navigation within the cislunar domain [44]. Additionally, the Air Force Research Laboratory (AFRL) is funding the Cislunar Highway Patrol System (CHPS) with the goal of deploying a remote sensing platform to monitor the vicinity of the Moon [16], [45].

2.7 Scheduling

This investigation seeks to build a scheduler for a cislunar R3 network to make deliveries to GEO satellites which optimizes the tradeoff between TOF and ΔV costs of high-thrust and low-thrust trajectories. Since this is a scheduling problem, a brief foray into scheduling theory is in order. Broadly speaking, scheduling is the study of assigning resources to complete a task most efficiently [46]. Scheduling has many disciplines, but this investigation appears to closely resemble a job shop scheduling problem (JSSP).

In the classic JSSP, there is a certain number of different workstations—sometimes referred to as machines in the literature—which each complete a different, individual job. Each workstation can only complete one job at a time and must complete the entire job before the workstation can become available to complete another job. The goal of the classical JSSP is typically to minimize the time it takes to complete all the jobs [47]; however, this will not be the case in the scenario of this investigation. The goal of this investigation and the subsequent JSSP is to minimize deviations and the penalties of those deviations from the schedule, making it a JSSP with scheduling criteria similar to that described by Jones [46].

The JSSP for this investigation will require servicing vehicles be brought to satellites in GEO. In this scenario the servicing vehicle itself is the workstation. There will be three different types of servicing vehicles: replacement vehicles which wholly replace defunct satellites in a constellation, repair vehicles which repair damaged satellites, and refueling vehicles which refuel by way of fully replacing the propellant tank with a full tank. The job will be considered to be the trajectory to get to the specified GEO node from one of the cislunar nodes—L_1 or DPO. The problem is defined in this manner since the trajectories to choose from will be either low-thrust or high-thrust trajectories and represent a significant trade-off in cost savings. The scheduler will be forced to choose between burning much more ΔV to minimize TOF and arrive in GEO quickly or minimize ΔV costs and use a trajectory with a much greater TOF. From these choices, the trajectory which minimizes the penalty for arriving either too early or too late will be selected.

There will be different penalties for deviation from arrival time depending on the vehicle type. It would be inefficient for a refueling vehicle to arrive to early and replace a propellant tank which is only half empty; however, it would be even more costly for a refueling vehicle to arrive too late and have the satellite either completely lost and require replacement or require a significant amount of fuel to return to orbit. If a satellite requires replacement, there clearly needs to be a criterion to deter premature arrival to avoid the outcome of over-congestion—an issue the scheduler is looking to solve. However, the replacement vehicle should also have a response-based demand in which there is no penalty for it arriving early since it is trying to replace a satellite as quickly as possible.

There will need to be a penalty for tardy replacement, since the critical systems supported by the GEO satellites in question cannot be put on hold. Clearly, a repair vehicle cannot arrive before a satellite is damaged so repair vehicles should have scheduled jobs as well as demand-based jobs. The repair vehicle will likely need to repair vehicles as quickly as possible to ensure efficient operation and should therefore not have a penalty for early arrival. Alternatively, the repair vehicle will have a penalty for tardy arrival since a late repair could jeopardize the functionality of the satellite. Once at the GEO node, the servicing jobs themselves will have one of three completion times based on the type of servicing vehicle.

There appears to be no literature at the time of writing on using the JSSP as a means for scheduling a satellite R3 network. However, in 2006, Barbulescu [48] used scheduling to deconflict requests for satellite access within the Air Force Satellite Control Network—known as the satellite range scheduling problem (SRSP). Barbulescu concludes that a genetic algorithm called *Genitor* is best suited for solving the SRSP for the historical demand on the network from 1992 to 2002-2003 [48].

The JSSP is often used operations research since the problem revolves around scheduling a finite amount of resources to accomplish a mission. Zhang et al. [49] studied flexible job shop scheduling problems (FJSSP) for various manufacturing systems. The FJSSP is analogous to the classical JSSP with the exception that the FJSSP allows an operation to be completed by any machine within a given set. All problems involved transportation constraints and processing constraints in which the handling of resources require upper and lower bounds—i.e. the resources need to be delivered before they deteriorate (the upper bound), but require a certain amount of time to be delivered (the

lower bound)—as well as constraints related to each specific problem. The FJSSP was found to be a suitable overarching model for the problems investigated.

Liu and Hsu [50] propose a job shop scheduling model which reduces due-date costs and minimizes earliness penalties in a dynamic job shop environment. In the investigation it is proposed that due-date costs per time unit and earliness penalties per time unit are not the same, as is commonly assumed in the traditional dispatching rules of JSSPs. Liu and Hsu [50], use three commonly used dispatch rules in JSSP and add nine novel dispatch rules which assume due-date costs per time unit and earliness penalties per time unit will have different values. It was found that dispatching rules simultaneously considering both the due-date costs per time unit and earliness penalties per time unit were far superior in minimizing total costs when compared to schemas using rules which considered just one of the two parameters. The investigation by Liu and Hsu [50] appears to be similar to the focus of the current investigation such that both investigations seek to minimize the penalties of off-time deliveries.

2.8 Hohmann Transfers

In this investigation, Hohmann transfers will be used to raise and lower orbits. The Hohmann transfer will be used because it is generally the most efficient way to transfer between coplanar orbits [51].The purpose of raising the orbit is to more efficiently change planes by making an inclination change at a greater altitude and therefore decrease ΔV costs, which will be discussed in later sections.

A Hohmann transfer is a coplanar maneuver, meaning the maneuver does not change the orbital plane. Only semimajor axis, eccentricity, and argument of perigee can

be altered during a coplanar transfer. Walter Hohmann in proposed 1925 that the transfer between two orbits which requires the minimum velocity could be achieved by using two tangential burns. This type of transfer later took on Hohmann's name and is now called the Hohmann Transfer.

Fig. 12 gives an example of a Hohmann transfer between two circular orbits. The first tangential burn, ΔV_a, occurs at perigee of the transfer orbit. ΔV_a increases the velocity of the satellite and raises the orbit. When the satellite reaches apogee of the transfer orbit, it applies a second tangential burn, ΔV_b, which decreases the velocity of the satellite. ΔV_b is in the opposite direction of ΔV_a and allows the satellite to exit the transfer orbit, entering the final targeted orbit. Calculating a Hohmann transfer is straightforward since the starting and ending positions are the initial and final radii and are the only two variables needed. The derivation of the Hohmann transfer will follow that of Vallado [51].

Starting with the initial and final positions, the semimajor axis of the transfer is found by:

$$a_{trans} = \frac{r_{initial} + r_{final}}{2} \tag{18}$$

The transfer velocities are then found using eq. 18.

$$v_{trans_a} = \sqrt{\frac{2\mu}{r_{initial}} - \frac{\mu}{a_{trans}}} \tag{19}$$

$$v_{trans_b} = \sqrt{\frac{2\mu}{r_{final}} - \frac{\mu}{a_{trans}}} \tag{20}$$

$$v_{intial} = \sqrt{\frac{\mu}{r_{initial}}} \tag{21}$$

$$v_{final} = \sqrt{\frac{\mu}{r_{final}}} \tag{22}$$

Where μ is the gravitational parameter of the Earth and the Moon. The ΔV's are then calculated by:

$$\Delta v_a = v_{trans_a} - v_{initial} \tag{23}$$

$$\Delta v_b = v_{final} - v_{trans_b} \tag{24}$$

$$\Delta v = |\Delta v_a| + |\Delta v_b| \tag{25}$$

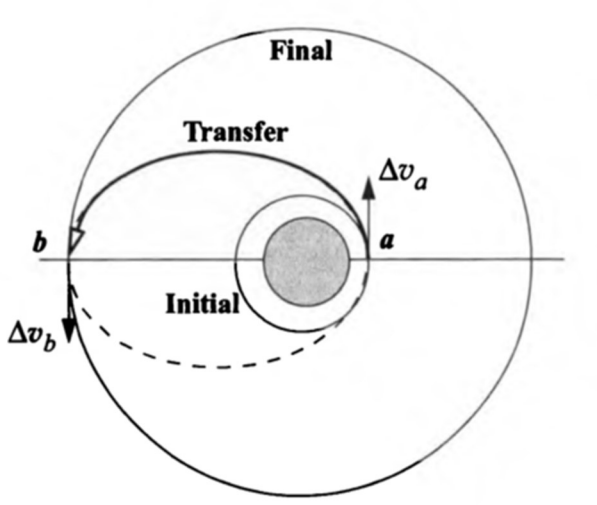

Figure 12: Example Hohmann transfer. Notice that the direction of the ΔVs are tangential to the orbit. Copied from [51]**.**

2.9 Inclination Changes

Inclination changes will be considered in this investigation for determining the arc costs of making deliveries to different nodes in GEO. An inclination change is one of the three types of noncoplanar maneuvers. A noncoplanar maneuver will change either inclination, right ascension of the ascending node, or both orbital elements. Inclination changes are typically used to position a satellite just after launch since the location of the launch site can limit what inclination the satellite can initially reach. As previously mentioned, only inclination changes will be considered in this investigation.

To change only inclination, the change must occur at an equator crossing within the orbit—i.e. at one of the nodes—since these points are the only two points common in both orbits. The GEOs considered in this investigation will only be circular, which greatly simplifies the ΔV calculation. During the inclination change the size of the orbit will not be changing and therefore the initial and final velocity vectors form an isosceles triangle with the change in inclination as the angle between the two velocity vectors. Following the derivation by Vallado [52]:

$$\sin\left(\frac{\Delta i}{2}\right) = \frac{\Delta V_{inc}}{2v_{initial}\cos(\phi_{fpa})} \tag{26}$$

Solving for the change in velocity yields:

$$\Delta V_{inc} = 2v_{initial}\cos(\phi_{fpa})\sin\left(\frac{\Delta i}{2}\right) \tag{27}$$

Where ΔV_{inc} is the ΔV required for the inclination change, ϕ_{fpa} is the flight path angle, $v_{initial}$ is the initial velocity, and Δi is the change in inclination. Note that when orbiting at lower altitudes the satellite will have a greater velocity than a satellite at a higher altitude. Therefore, a satellite at a lower altitude will require a greater ΔV_{inc} since

the initial velocity will be greater. Satellites at a higher altitude will have a lower initial velocity and therefore require less ΔV to change inclination

2.10 Summary of contributions

The goal of this investigation was originally to create a scheduler which minimized deviations from a provided schedule of required R3 delivery dates by inclination and RAAN. In order to achieve this an ED-GMCNF was needed. Collins' research [11] provided an ED-GMCNF framework for high-thrust trajectories. It was planned in this research to first augment the model created by Collins to include low-thrust vehicles and additional nodes. Then a dynamic scheduler leveraging this model would be built. This investigation resulted in three main contributions:

- Contribution 1: Initial trajectory results of high-thrust vehicles during the creation of this augmented ED-GMCNF indicated that regardless of whether the trajectories leaving L_1 were ΔV optimized or TOF optimized, the difference in TOF was trivial as compared to model assumptions.
- Contribution 2: The results from contribution 1 indicated a pivot in investigative focus was appropriate. As such, the second contribution was an investigation into the ΔV optimal trajectories from L_1 and a DPO to various GEO inclinations. It was found that trajectories from the DPO may offer significant savings in ΔV.
- Contribution 3: Further investigation was performed to minimize the ΔV costs of inclination changes in GEO for the purpose of servicing multiple GEO satellites. This resulted in finding it is most ΔV-efficient to Hohmann transfer to a greater radius of GEO when starting above the equatorial plane (0º of inclination) as

opposed to simply performing the inclination change at the starting radius. More ΔV is saved by completing the inclination change at a greater radius of GEO than is spent in transferring to that radius. The most ΔV-efficient radius found in this investigation is 1.25xGEO (52,705 km) unless maneuvering through 90º of inclination in which case it is most efficient to transfer to a radius 3xGEO (126,492 km). When beginning in the equatorial plane, remaining at a GEO radius of 42,164 km was most efficient unless maneuvering through 90º of inclination.

III. Methodology

Chapter Overview

This chapter of the investigation will address how the investigation itself was structured. The chapter will begin with the initial investigative focus and the original research questions. The original assumptions will then be stated before covering the negative results of the original investigation which led to a change in the approach of the investigation. The revised investigative focus is then explained, and the new research questions are stated.

3.1 Initial Investigation Methodology

The original focus of this investigation was to expand on previous work [11] by formulating an optimal delivery scheduler of both high-thrust and low-thrust refueling, repair, and replacement (R3) vehicles to circular geosynchronous orbits (GEOs) with a semi-major axis of 42,164 km. These refueling vehicles would be parked in Lyapunov orbits around the Earth-Moon L_1 Lagrange point (L_1). The L_1 orbit used in this investigation is the same used in the investigation by Collins [11]. From the parking orbits, a comparison would be made between trajectories which minimize either ΔV or time-of-flight (TOF) to find the optimal solutions of the schedulers. Once the trajectories had been completed, the next goal was to incorporate additional cislunar orbits—such as halo orbits and distant retrograde orbits (DROs)—to compare station-keeping costs.

With inclusion of DROs, the station-keeping costs would be compared between the L_1 orbits and the DROs. This would determine if it is optimal to spend the fuel to get to the DRO and take advantage of the lower station-keeping costs despite the time cost of

being in such a long-period orbit. From these parking orbits, the spacecraft would transfer and inject into GEO at various inclinations.

The high-thrust trajectories were originally built for Collins' [11] investigation using Analytical Graphics Inc.'s (AGI) Systems Tool Kit (STK) software. STK's Sparse Nonlinear OPTimizer (SNOPT) and differential corrector tools were used to collect the ΔV and TOF data of the trajectories[2]. The trajectories from Collins' investigation were modified for this investigation to target various inclinations using the same setup. An example of a high-thrust trajectory from L_1 to GEO can be seen in Fig. 13. The ΔV and TOF data of the low-thrust trajectories were to be collected using the Gauss Pseudospectral Optimization Software (GPOPS) for MATLAB. However, due to time constraints, data could not be collected for the low-thrust trajectories.

[2] Please refer to Appendix A for more information on the SNOPT and how the trajectories were modified in STK.

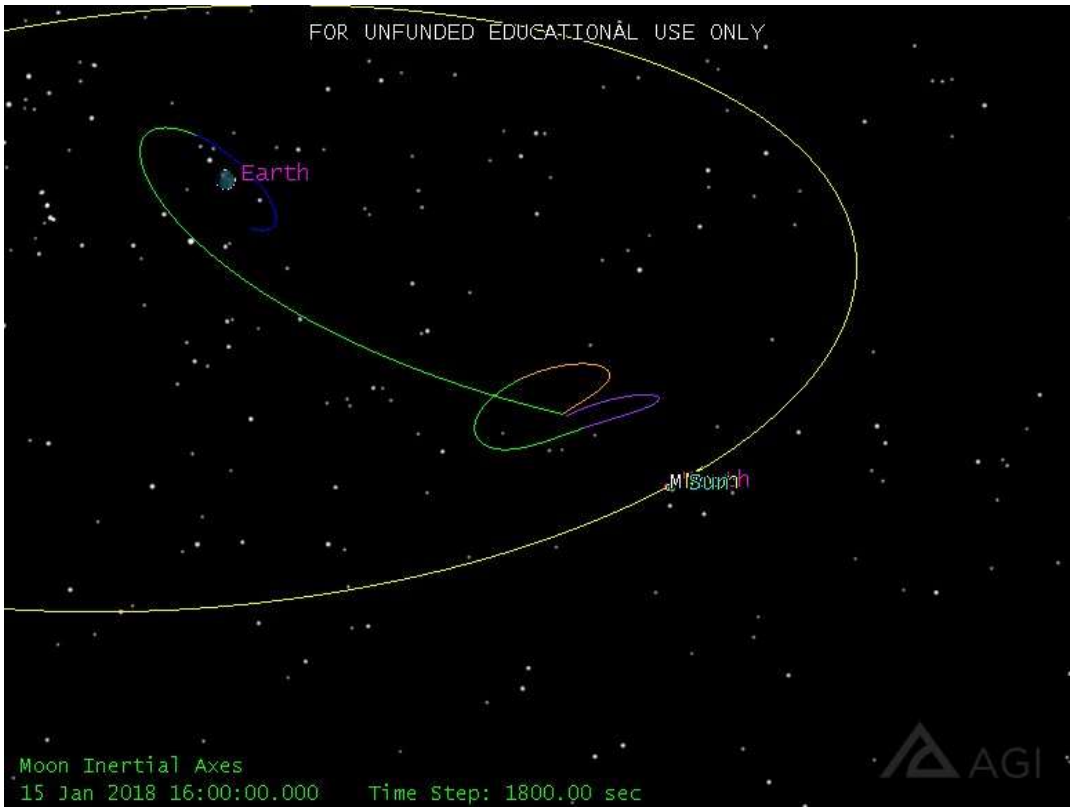

Figure 13: Example trajectory from L_1 to GEO. Recorded from STK.

The ΔV and TOF data would then be used to create the costs associated with each arc of the ED-GMCNF. Nodes of the network would be placed at:

- Specific values of inclination and right ascension of the ascending node (RAAN) in GEO
- The Kennedy Space Center
- The L_1 Lagrange point
- The Lunar surface
- Low Lunar Orbit

DROs and Halo orbits would have been included in the investigation as nodes given adequate time to construct the trajectories and test the network with these added

nodes. The commodities being transported across this network would follow Collins' work [11] and consist of:

- Propellant for refueling
- Replacement satellites
- Service vehicles
- Launch vehicle

Each commodity is defined by its mass, so using the ΔV associated with each arc would then determine the fuel cost associated with the movement of each commodity across the network through the ideal rocket equation:

$$\frac{m_{propellant}}{m_{dry}} = \exp\left(\frac{\Delta V}{I_{sp} g_0}\right) \tag{28}$$

Where I_{sp} is the specific impulse of the propulsion system and g_0 is the standard gravity acceleration at sea-level.

3.2 Initial Investigation Assumptions

- A required refueling schedule by inclination and RAAN would be available. Since no such schedule exists, several schedules would be randomly generated to test scheduler sensitivity to requirements.
- The network would be made dynamic by investigating the gravitational effects of the Moon. If the Moon's gravitational effects on cislunar trajectories vary with the time of the month, it would be advantageous for spacecraft to leave the vicinity of the Moon during different epochs. Therefore, the scenario would be tested at different time epochs separated

by at least three days to find the significance of the Moon's gravitational affect.

- The delivery vehicles would all have fixed starting masses, and each would carry a fixed amount of fuel.
- Each refueling delivery would deliver a fixed amount of fuel to each target satellite. This assumption is made without technological considerations as to how the fuel is physically delivered to the target.
- In GEO, the proximity and rendezvous operations of the satellites were assumed to be instantaneous.
- All fuel transported—as well as all propellant used—by the R3 vehicles was sourced via lunar ISRU. The fuel would be stored in a depot maintained in the L_1 Lyapunov orbit.
- High-thrust vehicles are able to use hydrogen-based propellants synthesized from lunar ice [11].
- It was assumed without technological consideration that the low-thrust vehicles would be able to source propellant through lunar ISRU. This assumption, however, may be weak as it is not well-supported by the literature [53] and is a key reason why low-thrust trajectories were left out of Collins' [11] investigation. There is the possibility that low-thrust engines could use liquid diatomic hydrogen as a propellant in a nuclear electric propulsion engine [53], but the development level and suitability of this type of engine is unclear.

- The vehicle is in the proper portion of the cislunar orbit to be able to maneuver and target a GEO inclination. This assumption pertains mostly to the DRO because of the length of the orbit period. Within the STK scenario the spacecraft completed a full Lyapunov orbit before starting for Earth.
- All arcs between nodes are assumed to be reversible, as was demonstrated by Whitley [25] and also assumed by Collins [11].

3.3 Initial Results of Original Methodology

High-thrust trajectories were built for the original investigation of an optimal delivery scheduler from L_1 to GEO. The trajectories were optimized by either minimizing ΔV or TOF. The SNOPT ran into issues selecting specific inclinations for the optimized trajectories. Trajectories continually could not be found between L_1 and GEO when targeting a specific trajectory. After talking to an engineer at AGI, it became apparent that the SNOPT was being over-constrained between minimizing either ΔV or TOF while selecting an inclination between the specified bounds of 1º. The software could not find trajectories in the solution space with such tight bounds. Thus, the original goal of selecting specific GEO inclination and RAAN values to inject into had to be modified. Since there were issues with selecting specific inclinations, the parameters were opened-up marginally within the SNOPT to allow selection of inclinations within bands of 15°. To take further pressure off of the SNOPT, retrograde GEOs were eliminated so that only bands of inclination between 0° and 90° could be targeted. After further issues with modeling cislunar trajectories within STK—see appendix B for details—the RAAN

parameters were opened to be between 0° and 180° and 180° and 360° before eliminating the RAAN requirement altogether. Eliminating the RAAN requirement proved to decrease the constraints enough to allow the SNOPT to find trajectories connecting to inclinations within the specified bounds.

Once the issue of finding trajectories to GEO inclinations was remedied, it was noted that the SNOPT still appeared to be over-constrained. Within the inclination bands, the SNOPT had two issues which appeared to be related to over-constraining. The SNOPT was either choosing the same trajectory, regardless of whether it was set to minimize TOF or ΔV, or the TOF difference between the two trajectories was very small. Such a small variation between trajectory values indicates only a small number of feasible solutions exists.

A summary of the results of the initial trials can be seen in Table 1. The standard deviation of TOF between the trajectories was 1.4 days, but the average TOF for the entire trajectory including the maneuver to exit L_1, change inclination and travel to GEO, and then circularize the orbit within GEO was 23.8 days. This suggests there are some TOF savings during the actual trip between the Earth and the Moon; however, when compared to the variance in TOF associated with the assumptions surrounding the period of the cislunar orbits, these savings are not significant. As a result of the lack of variability in TOF between arcs, it was concluded that the initial investigative question was no longer valid.

Table 1: Statistics on Direct Trajectories to GEO from L1

	Avg	Median	Min	Max	Standard dev
Delta V (m/s)	2358	2325	1587	3774	620
Duration (days)	24.7	25.0	21.6	28.2	1.4

3.4 Revised Investigation Methodology

Upon noticing that the deviation in ΔV was greater than 25% of the average ΔV of trajectories leaving L_1 for GEO, the focus of the investigation was shifted. As such, the new investigative questions became:

1. What delivery arcs within an ED-GMCNF require the least ΔV?
2. If the delivery vehicle were to deliver to multiple GEO inclinations, where should the inclination changes be made to minimize ΔV?

To answer these questions, the trajectories previously made connecting the L_1 Lyapunov orbit to the inclination bands within GEO were used and many plane change maneuvers were created.

The effect of orbit radius on plane change costs were investigated by modeling inclination changes within STK. The inclination changes took place at several multiples of GEO: 1x, 1.25x, 1.5x, 1.75x, 2x, 2.5x, and 3xGEO (42,164 km, 52,705 km, 63,246 km, 73,787 km, 84,328 km, 105,410 km, 126,492 km respectively). The plane change at 1xGEO is simply a pure inclination change with no Hohmann transfer to serve as a base case scenario to compare ΔV costs. Within STK this plane change was done using a differential corrector targeting sequence. All other plane changes included a burn using the SNOPT to raise the orbit to the respective multiple of GEO; an inclination change combined with a circularization maneuver using the SNOPT to minimize ΔV costs; a

burn to lower the orbit back to GEO; and finally, a burn to circularize the orbit. Fig. 14 displays an example of the inclination changes.

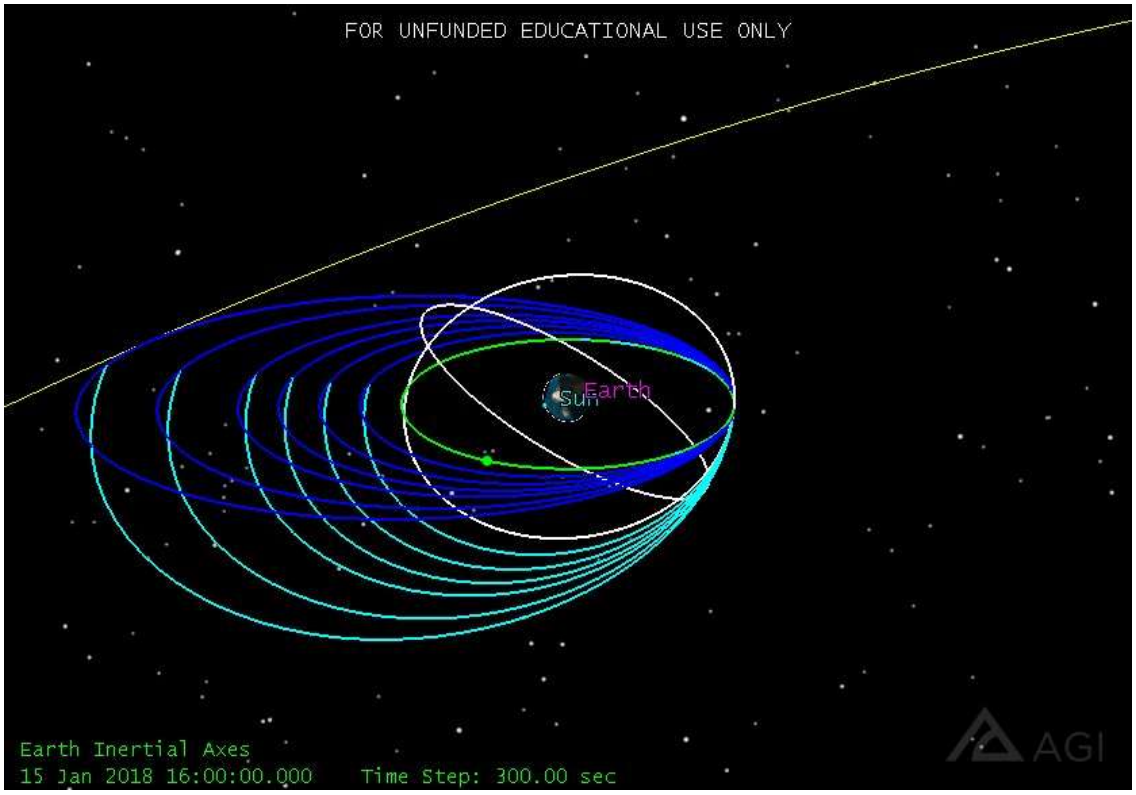

Figure 14: 30 degree inclination change with all multiples of GEO radius displayed. Recorded from STK.

Additional trajectories from a Distant Prograde Orbit (DPO) with a distance of 93,826 km from the Moon were also added for comparison to the trajectories from L_1. The DPO trajectory was developed and used in Collins' investigation [11], but were deemed suitable for the current investigation. It would be interesting and possibly of great utility to investigate how costs vary across the family of DPOs in future investigations. Unfortunately in this investigation, STK could only find trajectories using a differential

corrector and therefore the ΔV costs are not optimized using the SNOPT. An example of the trajectories from DPO to GEO can be seen in Fig. 15.

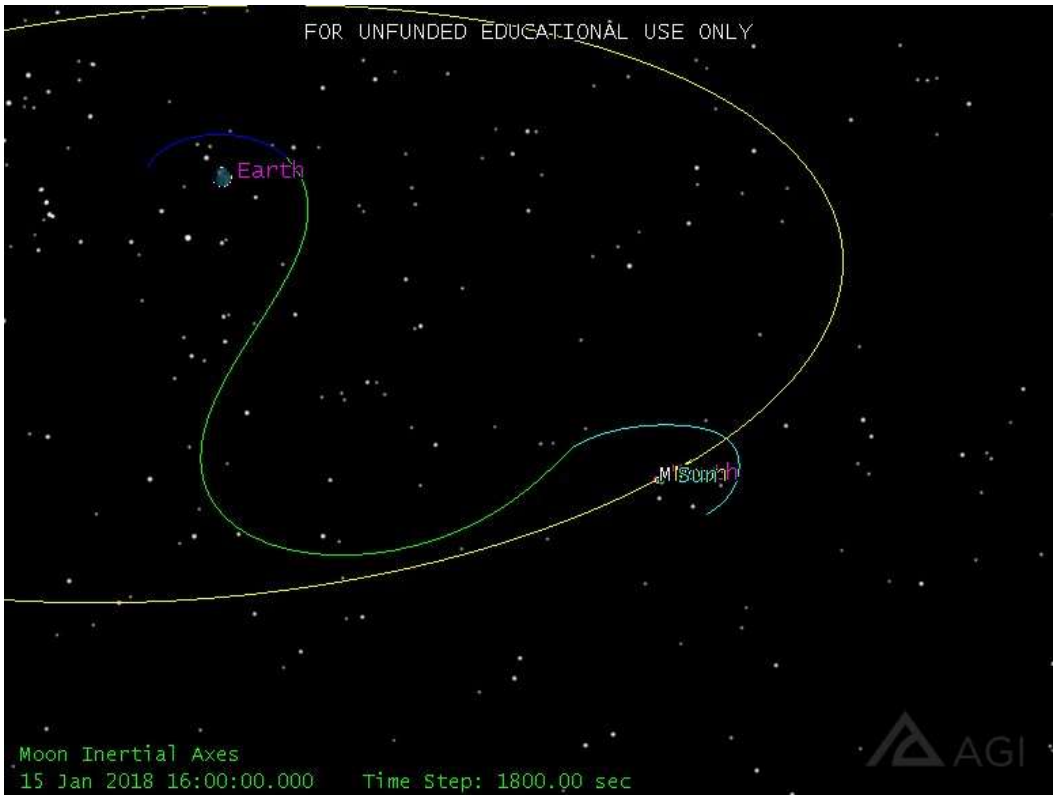

Figure 15: Example trajectory from DPO to GEO. Recorded from STK.

The ΔV costs and TOF data found in the investigation provide the costs to travel across arcs connecting the nodes of an ED-GMCNF as described previously. Future works looking to include these values in an ED-GMCNF will need to ensure the ΔV costs do not vary with the gravitational epoch of the Moon. The position of the Moon may alter the geometry of the greater Earth-Moon-Sun system and have a notable effect on ΔV costs. Due to time constraints the ED-GMCNF could not be formulated for this investigation.

IV. Analysis and Results

Chapter Overview

This Chapter describes the results gathered from Analytical Graphics Inc.'s (AGI) Systems Tool Kit (STK) software and offers an interpretation of the data gathered. Section 4.1 investigates the ΔV costs of trajectories connecting L_1 or DPO to GEO and describes contribution 2 of this investigation. Section 4.2 investigates the ΔV costs of making multiple servicing deliveries to different inclinations of GEO and describes contribution 3 of this investigation.

4.1 Trajectories from L1 and DPO to GEO

Table 2 shows the results of the trajectories from L_1 to geosynchronous orbit (GEO) as generated by STK. Each trajectory is grouped into 15° bands of inclination equally dividing the range of 0-90°. As described in the methodology section, inclination bands of 15° were selected since STK's Sparse Nonlinear Optimizer (SNOPT) could not find trajectories which minimize either ΔV or time-of-flight (TOF) when targeting specific inclinations. The band size of 15° was also selected in the hopes that it would provide enough variation between each band while still providing different trajectories to provide meaningful data.

Many of the trajectories selected by the SNOPT for minimizing ΔV have greater—or very similar—ΔV costs than the trajectories minimizing TOF; and many of the trajectories minimizing TOF have very similar TOFs to the trajectories minimizing ΔV. Having such little variation across the population of optimal trajectories indicates the system is over-constrained and therefore has a small solution space. With such a small

solution space, the SNOPT can only pick between a few trajectories resulting in solutions with a high degree of similarity despite the optimization criteria.

Since the SNOPT appears to be over-constrained, the average values of the trajectories in each inclination band were taken and a summary of the average statistics are displayed in Table 3. Table 3 also shows that the trajectories to the 15-30° inclination band have the lowest ΔV costs on average. This inclination band also includes the lowest minimum and maximum ΔV costs. These statistics appear to indicate that trajectories to the 15-30° inclination band offer the lowest ΔV costs overall. These ΔV savings make sense since the Moon is inclined to the Earth's equatorial plane. The Moon's inclination with respect to the Earth slowly changes over time between a minimum of 18° and a maximum of 28°.

The purpose of the averaged ΔV and time-of-flight (TOF) values from Table 3 is to provide the arc costs for high-thrust vehicles to travel from the L_1 node to each inclination node in GEO as part of an event-driven generalized commodity network flow (ED-GMCNF). The focus of this investigation was to develop an ED-GMCNF which models a cislunar network scheduler for GEO satellite refueling, repair, and replacement (R3). High-thrust and low-thrust vehicles would be compared to find optimality for the system. Due to time constraints, trajectories for the low-thrust vehicles could not be developed and therefore the ED-GMCNF could not be formulated.

Table 4 displays the TOF and ΔV data of trajectories of spacecraft exiting a distant prograde orbit (DPO) with a semi-major axis of 91,826 km about the Moon and targeting inclinations in GEO. The trajectories leaving DPO for GEO appear to offer significant savings in both TOF and ΔV when compared to the trajectories leaving L_1 for

GEO and are displayed in Table 5. On average the DPO saves 9 days in TOF and 816 m/s in ΔV, totaling to 42% and 41% savings respectively. These savings are likely caused by the spacecraft leaving the DPO at the point in the orbit which is closest to Earth after completing only a small portion of the orbit. However, the trajectories leaving L_1 need to complete a full orbit before maneuvering to target GEO as part of construction of the scenario. The L_1 orbit was originally created by Collins [11] using the work of Brick [20], Dahlke [54], and Ostman [13]. It leaves at the optimal point in the periodic orbit so as to minimize energy. Requiring a full orbit also accounts for any variation for when a space vehicle may be tasked to maneuver from the orbit for a job. As previously noted, DPOs are very large so there is likely significant variation in the values of the trajectories leaving the orbit depending on where in the orbit the spacecraft is. Finally, the values displayed in Table 4 were found using STK's differential corrector and may not be the optimal solutions. The TOF and ΔV costs displayed in Tables 2-4 are assumed to be reversible.

Table 2: Statistics of Trajectories from L_1 to GEO

This table organizes the trajectories selected by the SNOPT into the defining bands of inclination which will serve as nodes of the ED-GMCNF in GEO. In the trajectory column the inclination selected by the SNOPT is given.

Inclination band	Trajectory	Minimized Parameter	TOF (days)	dV (m/s)
0-15 deg	L1 to GEO, 5 inc	dV	22.19	3085
	L1 to GEO, 5 inc	TOF	24.81	1733
	L1 to GEO, 8 inc	dV	24.34	2794
	L1 to GEO, 10 inc	TOF	24.82	1606
15-30 deg	L1 to GEO, 15 inc	dV	25.31	1587
	L1 to GEO, 15 inc	TOF	25.31	1588
	L1 to GEO, 30 inc	dV	25.24	2325
	L1 to GEO, 30 inc	TOF	25.24	2324
30-45 deg	L1 to GEO, 35 inc	dV	25.22	2344
	L1 to GEO, 40 inc	dV	25.21	2364
45-60 deg	L1 to GEO, 45 inc	dV	25.31	1972
	L1 to GEO, 45 inc	TOF	25.31	1972
	L1 to GEO, 54 inc	TOF	21.57	3564
60-75 deg	L1 to GEO, 60 inc	dV	28.18	2412
	L1 to GEO, 60 inc	TOF	24.54	2150
	L1 to GEO, 64 inc	dV	24.98	2426
	L1 to GEO, 64 inc	TOF	24.98	2426
	L1 to GEO, 68 inc	dV	25.23	1713
75-90 deg	L1 to GEO, 80 inc	TOF	24.89	2241
	L1 to GEO, 89 inc	dV	24.95	3112
	L1 to GEO, 84 inc	TOF	21.66	3774

Table 3: Summary of Average Statistics of Trajectories from L_1 to GEO

Here the averages within each band from Table 2 are displayed. These are the arc costs to travel from L_1 to each GEO node. Note that the 15-30º band has the lowest ΔV costs.

Inclination band	Avg TOF (days)	Min TOF (days)	Max TOF (days)	Avg dV (m/s)	Min dV (m/s)	Max dV (m/s)
0-15 deg	24.0	22.2	24.8	2304	1606	3085
15-30 deg	25.3	25.2	25.3	1956	1587	2325
30-45 deg	25.2	25.2	25.2	2354	2344	2364
45-60 deg	24.1	21.6	25.3	2502	1972	3564
60-75 deg	25.6	24.5	28.2	2225	1713	2426
75-90 deg	23.8	21.7	24.9	3042	2241	3774

Table 4: Statistics of Trajectories from DPO to GEO

This table displays the arc costs to travel from the DPO node to the nodes at GEO. Note that the average appears to give significant savings when compared to the L_1 arc costs in Table 3.

Targeted Inclination	TOF (days)	dV (m/s)
10 degrees	13.4	1317
20 degrees	15.3	1437
35 degrees	16.9	1568
50 degrees	17.5	1660
65 degrees	17.3	1729
80 degrees	16.3	1777
Average	**16.1**	**1582**

Table 5: Savings of DPO vs. L_1

This table displays the savings of the arcs from the DPO node to GEO vs. L_1 node to GEO.

Inclination band	TOF Difference (days)	TOF Percent Difference	dV Difference (m/s)	dV Percent Difference
0-15 deg	11	57%	987	55%
15-30 deg	10	49%	519	31%
30-45 deg	8	39%	786	40%
45-60 deg	7	31%	842	40%
60-75 deg	8	39%	496	25%
75-90 deg	7	37%	1265	52%
Average:	**9**	**42%**	**816**	**41%**

4.2 Inclination Changes in GEO

As previously mentioned, a number of inclination changes were modeled at various multiples of GEO altitude to gather data on the TOF and ΔV costs of such maneuvers. Various inclination changes would be necessary for a vehicle making multiple deliveries within GEO after traveling from one of the cislunar nodes (L_1 or DPO). This is necessary to understand whether it is most efficient to stay in GEO after a delivery or to return to cislunar space to resupply and make another delivery. The data from the inclination changes in Tables 6-11 serves as the TOF and ΔV costs to travel between the nodes within GEO—with each node being placed at the inclination bands—of the originally planned ED-GMCNF between the Earth and cislunar orbits.

Inclination changes were done at multiples of GEO altitude to understand the affects altitude has on the ΔV costs of inclination changes. Once the effect of altitude is understood, it is possible to determine the most advantageous distance from Earth at which to make an inclination change. The advantage will depend on whether TOF or ΔV must be conserved in the missions of the ED-GMCNF. The costs of each inclination

change were further broken down into the ΔV cost for the inclination change itself and the ΔV cost for the Hohmann transfer to maneuver to the targeted multiple of GEO altitude. The column named *Total dV*, is the sum of the *Plane Change dV* and *Hohmann Transfer dV*. This was done to show the ΔV trade-off of using a Hohmann transfer to decrease the cost of the inclination change. As expected, the greater the multiple of GEO at which the inclination change was performed, the less ΔV costly the inclination change.

In general, when starting at the equatorial plane (i.e. 0° of inclination), it is least costly in both TOF and ΔV to remain at 1xGEO and make the inclination change directly. This trend continues (Tables 6-11, inclination changes 0-15°, 0-30°, 0-45°, 0-60°) until the more extreme inclination changes of 75° and 90° (Tables 10 and 11, inclination changes 0-75° and 0-90°). When starting above the equatorial plane (for example an inclination change from 15-30°, etc.), maneuvering to a multiple of 1.25xGEO radius becomes most ΔV efficient for inclination changes. This trend continues through all inclination changes where the starting inclination is above 0° (Tables 6-10). It appears there are no meaningful ΔV savings to be had between maneuvering to different radii in the inclination change from 0° to 75°. Instead, it is likely most effective to take advantage of the shorter TOF by maneuvering at 1xGEO. When maneuvering through a total of 90° of inclination, the savings of changing inclination at a greater radius are so great that it becomes efficient to spend ΔV to maneuver to a multiple of 3xGEO.

To further investigate the trend of ΔV savings at the equatorial plane, the inclination change from 0-15° was broken down into increments of 3°. This was done to determine at what inclination above the equatorial plane the trend discontinues. As can be seen in Table 12, the trend of ΔV savings stops when changing from 6-9° of inclination.

At this increment, it becomes more ΔV efficient to reap the benefits of the less costly inclination change at 1.25xGEO by spending the ΔV required to complete the Hohmann transfer. However, the ΔV savings does come at the cost of a greater TOF which is an important cost factor within an ED-GMCNF.

A trend in the data is that while inclination changes themselves require less ΔV at greater multiples of GEO radius, the ΔV cost to complete the Hohmann transfer to get to that greater radius starts to outweigh the savings. It is not until the extreme inclination change through 75° of inclination (15-90°) where this trend starts to reverse. The ΔV cost of such extreme inclination changes becomes so high that it begins to outweigh the cost of the Hohmann transfer to a greater multiple of GEO radius. With the exception of the 90° inclination change, it is advantageous in this scenario to Hohmann transfer to 1.25xGEO altitude to minimize total ΔV costs; however, if starting at the equatorial plane a direct transfer will be most efficient. Further investigation is needed to determine if the point of optimality lies between a 1 or 1.25 multiple of GEO radius.

Table 6: 15 Degree Inclination Changes

The costs of inclination changes through 60º of inclination are displayed. Total ΔV of the maneuver is broken up into its constituents. A Hohmann transfer to 1.25xGEO radius is most efficient when starting above the equatorial plane. Minimum values are bolded.[3]

Inclination change	XGEO	Total dV (m/s)	Plane Change dV (m/s)	Hohmann Transfer dV (m/s)	TOF (days)
0 to 15	**1**	**808**	**808**	**0**	**1.6**
	1.25	1203	714	489	4.7
	1.5	1524	673	851	5.1
	1.75	1785	655	1130	5.5
	2	1998	648	1349	6.0
	2.5	2320	646	1674	6.9
	3	2549	646	1903	7.9
15 to 30	1	2250	2250	0	1.6
	1.25	**1203**	**714**	**489**	**4.2**
	1.5	1525	674	852	4.4
	1.75	1786	656	1129	4.6
	2	1999	650	1349	4.8
	2.5	2322	648	1674	5.3
	3	2552	650	1901	5.8
30 to 45	1	3592	3592	0	1.6
	1.25	**1203**	**714**	**489**	**4.2**
	1.5	1525	674	852	4.4
	1.75	1785	656	1129	4.6
	2	1999	649	1350	4.8
	2.5	2322	648	1674	5.3
	3	2551	650	1901	5.8
45 to 60	1	4735	4735	0	1.6
	1.25	**1203**	**714**	**489**	**4.2**
	1.5	1525	673	852	4.4
	1.75	1786	656	1130	4.6
	2	1999	649	1350	4.8
	2.5	2322	648	1675	5.3
	3	2551	650	1901	5.8
60 to 75	1	5587	5587	0	1.6
	1.25	**1203**	**714**	**489**	**4.2**
	1.5	1525	673	852	4.4
	1.75	1785	656	1129	4.6
	2	1999	649	1350	4.8
	2.5	2322	648	1674	5.3
	3	2551	650	1901	5.8
75 to 90	1	6075	6075	0	1.6
	1.25	**1203**	**714**	**489**	**4.2**
	1.5	1525	673	852	4.4
	1.75	1786	656	1130	4.6
	2	1999	649	1350	4.8
	2.5	2322	648	1674	5.3
	3	2550	649	1901	5.8

[3] The inclination changes done at GEO should technically be instantaneous and therefore have a TOF of zero. However, to properly set up the inclination change in STK, it is necessary to include a propagate to apoapsis segment at which to make the inclination change. Instead of manipulating the data, the results were taken directly from STK and not edited other than rounding.

Table 7: 30 Degree Inclination Changes

The costs of inclination changes through 30º of inclination are displayed. Total ΔV of the maneuver is broken up into its constituents. A Hohmann transfer to 1.25xGEO radius is most efficient when starting above the equatorial plane. Minimum values are bolded.

Inclination change	XGEO	Total dV (m/s)	Plane Change dV (m/s)	Hohmann Transfer dV (m/s)	TOF (days)
0 to 30	**1**	**1592**	**1592**	**0**	**1.6**
	1.25	1879	1390	489	4.7
	1.5	2108	1256	852	5.1
	1.75	2291	1161	1130	5.5
	2	2440	1091	1349	6.0
	2.5	2668	994	1674	6.9
	3	2831	928	1903	7.9
15 to 45	1	2990	2990	0	1.6
	1.25	**1880**	**1391**	**489**	**4.2**
	1.5	2109	1257	852	4.4
	1.75	2292	1162	1129	4.6
	2	2441	1092	1349	4.8
	2.5	2670	996	1674	5.3
	3	2833	931	1901	5.8
30 to 60	1	4233	4233	0	1.6
	1.25	**1880**	**1391**	**489**	**4.2**
	1.5	2108	1391	718	4.4
	1.75	2291	1162	1129	4.6
	2	2442	1092	1350	4.8
	2.5	2669	995	1674	5.3
	3	2832	931	1901	5.8
45 to 75	1	5231	5231	0	1.6
	1.25	**1880**	**1390**	**489**	**4.2**
	1.5	2108	1257	852	4.4
	1.75	2291	1162	1130	4.6
	2	2442	1092	1350	4.8
	2.5	2669	995	1675	5.3
	3	2832	931	1901	5.8
60 to 90	1	5587	5587	0	1.6
	1.25	**1879**	**1390**	**489**	**4.2**
	1.5	2108	1256	852	4.4
	1.75	2292	1162	1130	4.6
	2	2441	1091	1350	4.8
	2.5	2669	995	1674	5.3
	3	2832	930	1901	5.8

Table 8: 45 Degree Inclination Changes

The costs of inclination changes through 45º of inclination are displayed. Total ΔV of the maneuver is broken up into its constituents. A Hohmann transfer to 1.25xGEO radius is most efficient when starting above the equatorial plane. Minimum values are bolded.

Inclination change	XGEO	Total dV (m/s)	Plane Change dV (m/s)	Hohmann Transfer dV (m/s)	TOF (days)
0 to 45	**1**	**2350**	**2350**	**0**	**1.6**
	1.25	2538	2049	489	4.7
	1.5	2687	1835	852	5.1
	1.75	2807	1677	1130	5.5
	2	2904	1555	1349	6.0
	2.5	3051	1377	1674	6.9
	3	3155	1253	1903	7.9
15 to 60	1	3672	3672	0	1.6
	1.25	**2539**	**2049**	**489**	**4.2**
	1.5	2688	1836	852	4.4
	1.75	2807	1678	1129	4.6
	2	2904	1555	1349	4.8
	2.5	3052	1378	1674	5.3
	3	3156	1255	1901	5.8
30 to 75	1	4792	4792	0	1.6
	1.25	**2538**	**2049**	**489**	**4.2**
	1.5	2687	1836	852	4.4
	1.75	2807	1677	1129	4.6
	2	2905	1555	1350	4.8
	2.5	3052	1378	1674	5.3
	3	3156	1254	1901	5.8
45 to 90	1	5628	5628	0	1.6
	1.25	**2538**	**2049**	**489**	**4.2**
	1.5	2688	1836	852	4.4
	1.75	2807	1677	1129	4.6
	2	2905	1555	1350	4.8
	2.5	3052	1378	1674	5.3
	3	3156	1254	1901	5.8

Table 9: 60 Degree Inclination Changes

The costs of inclination changes through 60º of inclination are displayed. Total ΔV of the maneuver is broken up into its constituents. A Hohmann transfer to 1.25xGEO radius is most efficient when starting above the equatorial plane. Minimum values are bolded.

Inclination change	XGEO	Total dV (m/s)	Plane Change dV (m/s)	Hohmann Transfer dV (m/s)	TOF (days)
0 to 60	**1**	**3009**	**3009**	**0**	**1.6**
	1.25	3163	2674	489	4.7
	1.5	3240	2388	852	5.1
	1.75	3302	2173	1130	5.5
	2	3353	2004	1349	6.0
	2.5	3429	1756	1674	6.9
	3	3481	1579	1902	7.9
15 to 75	1	4291	4291	0	1.6
	1.25	**3164**	**2674**	**489**	**4.2**
	1.5	3240	2389	852	4.4
	1.75	3303	2173	1130	4.6
	2	3353	2004	1349	4.8
	2.5	3430	1756	1674	5.3
	3	3481	1580	1901	5.8
30 to 90	1	5266	5266	0	1.6
	1.25	**3163**	**2674**	**489**	**4.2**
	1.5	3240	2388	852	4.4
	1.75	3302	2173	1129	4.6
	2	3354	2004	1350	4.8
	2.5	3430	1755	1674	5.3
	3	3481	1579	1902	5.8

Table 10: 75 Degree Inclination Changes.

Note that with the 0 to 75º inclination there is not a significant ΔV difference between staying at 1 GEO radius or maneuvering to 1.25xGEO radius. However, there is a significant TOF difference which will likely make the 1xGEO the more desirable radius. With the 15 to 90º inclination change, 1.25xGEO clearly saves the most ΔV. Lowest values are bolded.

Inclination change	XGEO	Total dV (m/s)	Plane Change Delta dV (m/s)	Hohmann Transfer dV (m/s)	TOF (days)
0 to 75	**1**	**3746**	**3746**	**0**	**1.6**
	1.25	**3744**	**3254**	**489**	**4.7**
	1.5	3754	2902	852	5.1
	1.75	3764	2635	1130	5.5
	2	3774	2425	1349	6.0
	2.5	3786	2113	1673	6.9
	3	3791	1889	1902	7.9
15 to 90	1	4831	4831	0	1.6
	1.25	**3744**	**3255**	**489**	**4.2**
	1.5	3754	2902	852	4.4
	1.75	3764	2635	1129	4.6
	2	3774	2425	1349	4.8
	2.5	3786	2112	1674	5.3
	3	3791	1889	1902	5.8

Table 11: 90 Degree Inclination Changes

Since inclination changes require so much ΔV, there are significant savings by maneuvering to 3xGEO radius to make such an extreme inclination change.

Minimum value is bolded.

Inclination change	XGEO	Total dV (m/s)	Plane Change dV (m/s)	Hohmann Transfer dV (m/s)	TOF (days)
0 to 90	1	4352	4352	0	1.6
	1.25	4268	3779	489	4.7
	1.5	4219	3367	851	5.1
	1.75	4184	3054	1130	5.5
	2	4156	2807	1349	6.0
	2.5	4112	2438	1673	6.9
	3	**4075**	**2173**	**1902**	**7.9**

Table 12: Breakdown of Inclination Changes Near Equatorial Plane.

This table finds the inclination above the equatorial plane at which it becomes more efficient to spend the ΔV to maneuver to a greater radius of GEO to save greater total ΔV. The bolded values indicate the cheapest maneuver.

Inclination change	xGEO	Total dV (m/s)	Plane Change dV (m/s)	Hohmann Transfer dV (m/s)	TOF (days)
0 to 3	**1x**	**162**	**162**	**0**	**1.6**
	1.25x	699	210	489	4.7
	1.5x	1143	292	852	5.1
	2x	1761	411	1350	6.0
3 to 6	**1x**	**452**	**452**	**0**	**1.6**
	1.25x	699	211	488	5.4
	1.5x	1144	293	851	5.8
	2x	1762	412	1350	6.7
6 to 9	1x	742	742	0	1.6
	1.25x	**699**	**211**	**488**	**5.4**
	1.5x	1144	293	851	5.8
	2x	1762	412	1350	6.7
9 to 12	1x	1031	1031	0	1.6
	1.25x	**699**	**211**	**488**	**5.4**
	1.5x	1144	293	851	5.8
	2x	1762	412	1350	6.7
12 to 15	1x	1324	1324	0	1.6
	1.25x	**699**	**211**	**488**	**5.4**
	1.5x	1144	293	851	5.8
	2x	1762	412	1350	6.7
15 to 18	1x	1611	1611	0	1.6
	1.25x	**699**	**211**	**488**	**5.4**
	1.5x	1144	293	851	5.8
	2x	1762	412	1350	6.7

V. Conclusions and Recommendations

5.1 Conclusions

This investigation sought to build off previous work to create an optimized delivery scheduler of a cislunar refueling, repair, and replacement (R3) network using in-situ resource utilization (ISRU) for Earth-orbiting satellites in geosynchronous orbit (GEO) by using an event driven generalized multi-commodity network flow (ED-GMCNF) to incorporate both high-thrust and low-thrust vehicles.

The original research questions could not be answered. Time-of-flight (TOF) values and ΔV values could only be collected for high-thrust trajectories from the cislunar nodes at the L_1 Lyapunov orbit (L_1) and the distant prograde orbit (DPO), leaving out halo orbits and distant retrograde orbits (DROs). The collection of data for the high-thrust trajectories required much more time than expected. The original investigation called for deliveries to specific inclinations. However, Analytical Graphics Inc.'s (AGI) Systems Toolkit (STK) often could not find optimal solutions for trajectories minimizing either ΔV or TOF. To give STK's sparse nonlinear optimizer (SNOPT) a greater solution space, the inclination parameters were increased to bands of 15° between 0-90° of inclination rather than target specific inclinations. This allowed the SNOPT to find what appeared to be feasible solutions.

After several trials it became apparent that there was a lack of variation between trajectories set to minimize ΔV and trajectories set to minimize TOF. However, it was noted that the standard deviation of ΔV was significant at about 26% of the average ΔV for all trajectories. From here the focus of the investigation changed to find:

1. Which delivery arcs of a hypothetical ED-GMCNF require the least ΔV?
2. If a delivery vehicle were to make deliveries to multiple GEO inclinations, where should the inclination changes be made to minimize ΔV

The resulting time constraint due to altering the focus of the investigation forced low-thrust trajectories to be left out of the investigation.

The average ΔV and TOF values of each trajectory from L_1 to each respective 15° inclination band was assigned as the arc cost for each respective trajectory. When the trajectories from L_1 are compared to the trajectories from the DPO, it appears the DPO has a significant advantage in both TOF and ΔV. However, this conclusion is limited by the design of the scenario within STK.

Firstly, the DPO trajectories were made using STK's differential corrector and therefore are not the optimal trajectories that would be found using the SNOPT as is the case with the L_1 trajectories. Secondly, the trajectories leaving L_1 require a full orbit before being in position to maneuver and target Earth whereas the vehicle leaving DPO completes only part of the DPO before maneuvering. A full DPO could not be modeled so it is unknown how great of an effect this would have on results. Realistically, a vehicle in a DPO would likely have a small window of optimality to maneuver and target Earth with minimal costs since the DPO has such a large orbit period. The cheapest DPO arc targets 10° of inclination, has a TOF of 13.4 days, and requires 1317 m/s of ΔV. The cheapest arc from L_1 targets the 15-30° inclination band, has a TOF of 25.3 days, and a ΔV cost of 1956 m/s.

To find where inclination changes must be made near GEO so as to minimize ΔV costs, all maneuvers between each inclination band were modeled. Each maneuver was done at multiples of 1x, 1.25x, 1.5x, 1.75x, 2x, 2.5x, and 3x GEO radius (42,164 km, 52,705 km, 63,246 km, 73,787 km, 84,328 km, 105,410 km, 126,492 km respectively). These trials indicated that when changing inclination from the equatorial plane (0° inclination) and the maneuver is less than a 75° change in inclination ΔV is minimized when maneuvering at a 1x multiple of GEO radius. When maneuvering through 75° of inclination 2 m/s of ΔV can be saved by using a Hohmann transfer to raise the orbit to 1.25xGEO radius and make the inclination change there. However, this will cost 4.7 days of TOF as opposed to the 1.6 days of TOF when staying at 1xGEO. Therefore, it is likely optimal to stay at 1xGEO for a maneuver from 0° to 75° of inclination. When maneuvering from an inclination above the ecliptic plane to another inclination, it was found that completing a Hohmann transfer to 1.25xGEO radius and then completing the inclination change before lowering the orbit always minimized ΔV costs.

Further research is needed to determine whether 1.25xGEO radius is the optimal radius at which to change inclination or if the point lies between 1.25xGEO and 1.5xGEO radius or between GEO and 1.25xGEO radius. If making multiple deliveries from L_1, it appears ΔV costs may be minimized by making inclination changes at Earth as opposed to returning to L_1 to target the second inclination before making the second delivery. However, this may not be the case for arcs between Earth and the DPO. An ED-GMCNF is required to determine optimality.

5.2 Future Work

This section will cover the recommendations for future work in the same area of cislunar research.

As described in earlier passages, a frequent problem in this investigation was getting trajectories from L_1 to converge. The SNOPT appeared to have issues finding optimal solutions when the bounds of targeted inclination became too small. It may be possible to explore the problem space further by altering the target sequence within STK or simply by using an optimizer other than the SNOPT. In the investigation, the space vehicle targeted inclination when it maneuvered to exit the Lyapunov orbit around L_1. Perhaps if the vehicle targeted inclination further along in the trajectory, STK could yield a higher fidelity in inclination selection.

Another area of this investigation which requires further exploration is the trajectories from DPO. Only a handful of trajectories connecting to each inclination band from a DPO of 91,826 km was used. Future works could incorporate multiple DPOs to find the optimal orbit size which minimizes TOF and ΔV of the incoming trajectories. Future investigations will also need to incorporate complete DPOs to test if there are other points within the orbit the vehicle should leave. A test of feasibility should also be incorporated for DPOs to determine if it is even feasible to use DPOs to store R3 vehicles due to their long orbital period. It needs to be found when it is reasonable to burn the ΔV to get to DROs to save station-keeping costs at the risk of the delivery vehicle being unavailable during demand. Additionally, the trajectories connecting the DPO to GEO in this investigation were not optimized. Further exploration is needed to build targeting sequences that the SNOPT can use to optimize trajectories.

Other cislunar orbits also need to be explored. The results of the trajectories used in this investigation could be compared against trajectories from other orbits such as halo orbit, near-rectilinear halo orbits, or distant retrograde orbits as well as the families of all of these orbits. Each orbit family has different characteristics when it comes to station-keeping costs, availability for agile support of Earth satellites, and occlusion from Earth communications.

Future works will also need to test whether or not the results of this investigation change with the Moon's gravitational epoch. Part of the original focus of this investigation was to find create a dynamic delivery scheduler. It is unknown if the position of the Moon within its orbit will have an effect on the optimality of the cislunar trajectories. For this investigation there was no simple way found to run the scenario at a different time epoch and it may require rebuilding the entire scenario at later epochs. Due to time constraints, this could not be achieved. With the incorporation of low-thrust trajectories and an understanding of how a changing gravitational epoch affects the arc costs found in this investigation, an ED-GMCNF could be built using the results of this investigation to help develop a dynamic scheduler.

Low-thrust trajectories are another area worthy of investigation. The ED-GMCNF framework was selected by the predecessor of this investigation because the ED-GMCNF can allow the inclusion of low-thrust trajectories by allowing the network flow to be duplicated at variable length time-steps. However, the question of whether low-thrust vehicles can be maintained via lunar ISRU still needs to be answered. If low-thrust vehicles can only be maintained by Earth-based means, it would violate the basic

assumption of this investigation that the R3 network can be self-sustaining in cislunar space.

A final recommendation for future work is to expand upon the results of this investigation with a higher-fidelity method to pinpoint the optimal multiple of GEO radius at which to make an inclination change. As demonstrated by the results of this investigation, there are significant savings in ΔV to be achieved by using a Hohmann transfer to raise the orbit of the satellite and then change inclination. The results of this investigation also appear to indicate the point of true optimality lies between GEO radius (42,164 km) and 1.5xGEO radius (63,246 km). Developing a method for—and finding—the GEO radius to transfer to and make an inclination change at which will minimize the total ΔV cost is likely an important finding for an ED-GMCNF considering multiple deliveries in GEO.

5.3 Contributions of this Research

The goal of this investigation was originally to create a scheduler which minimized deviations from a provided schedule of required R3 delivery dates by inclination and RAAN. In order to achieve this an ED-GMCNF was needed. Collins' research [11] provided an ED-GMCNF framework for high-thrust trajectories. It was planned in this research to first augment the model created by Collins to include low-thrust vehicles and additional nodes. Then a dynamic scheduler leveraging this model would be built. This investigation resulted in three main contributions:

- Contribution 1: Initial trajectory results of high-thrust vehicles during the creation of this augmented ED-GMCNF indicated that regardless of whether the

trajectories leaving L_1 were ΔV optimized or TOF optimized, the difference in TOF was trivial as compared to model assumptions due to the length of the Lyapunov orbit.

- Contribution 2: The results from contribution 1 indicated a pivot in investigative focus was appropriate. As such, the second contribution was an investigation into the ΔV optimal trajectories from L_1 and a DPO to various GEO inclinations. It was found that trajectories from the DPO may offer significant savings in ΔV.
- Contribution 3: Further investigation was performed to minimize the ΔV costs of inclination changes in GEO for the purpose of servicing multiple GEO satellites. This resulted in finding it is most ΔV-efficient to Hohmann transfer to a greater radius of GEO when starting above the equatorial plane. The most ΔV-efficient radius found in this investigation is 1.25xGEO unless maneuvering through 90º of inclination in which case it is most efficient to transfer to a radius 3xGEO. When beginning in the equatorial plane, remaining at a GEO radius of 42,164 km was most efficient unless maneuvering through 90º of inclination.

Appendix A

This appendix aims to communicate how the trajectories were modified in STK and how the sparse nonlinear optimizer (SNOPT) was used to modify trajectories. The SNOPT uses sequential quadratic programming to find locally optimal solutions [11]. The SNOPT works best when trying to target a trajectory which has already been calculated, such as by a differential corrector. The initial values need to be close to a possible solution for the SNOPT profile to converge. This may have been an area of error: the initial values given to the SNOPT may not have been close enough to a solution.

Since the SNOPT finds locally optimal solutions, it should be easier for the SNOPT to converge on a solution as more constraints are added. The more constraints there are, the smaller the search space the SNOPT must work through to find the optimal solution. In this investigation, however, once constraints were dropped and the targeting parameters opened up the SNOPT was able to find solutions. Again, this seems to point towards the initial values being given to the SNOPT were not close enough to a feasible solution. Once the parameters were opened up, the SNOPT may have taken longer to find an optimal solution in the larger search space, but eventually a solution was found since an optimal solution was now within the search space.

The trajectories to GEO from L_1 and the DPO were made by modifying the trajectories used by Collins [11]. This was done simply by editing the bounds on the targeted inclination (and RAAN value) within the SNOPT profile contained within the inclination change targeting sequence (Figs.16-17). The “Lower orbit” targeting sequence in the Fig. 16 is then optimized using the SNOPT to either minimize ΔV of the maneuver

or minimize the TOF of the trajectory to Earth. The SNOPT profile of the “Lower orbit” target sequence is shown in Fig. 18.

The DPO trajectory to GEO was modified in much the same manner as the L_1 trajectory to GEO. The targeting profile of the DPO is displayed in Fig. 19 and the parameters of the differential corrector are displayed in Fig. 20.

The inclination changes were created using the STK tutorials provided by AGI and are easily accessible online. Figs. 21-22 display the targeting profiles of the two methods of inclination change.

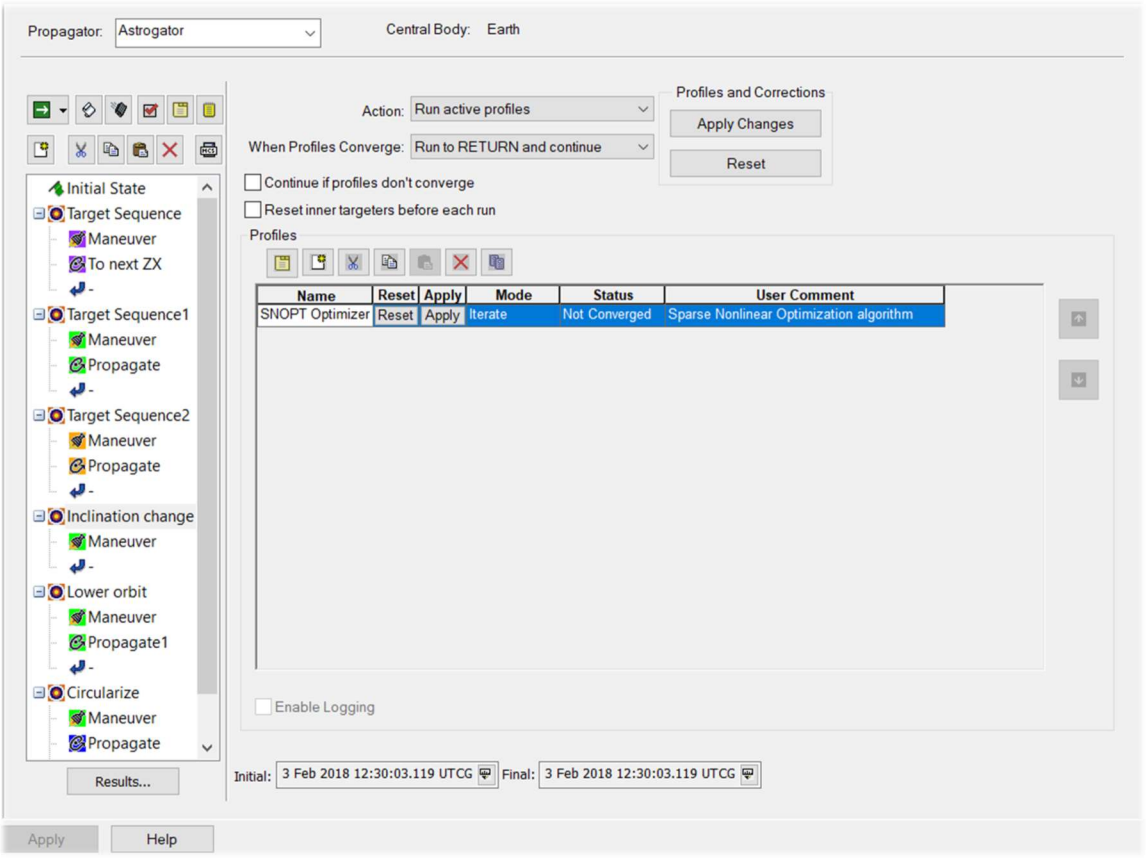

Figure 16: Targeting profile of the L_1 trajectory to GEO. Only the "Inclination change" and "Lower orbit" targeting sequences use the SNOPT.

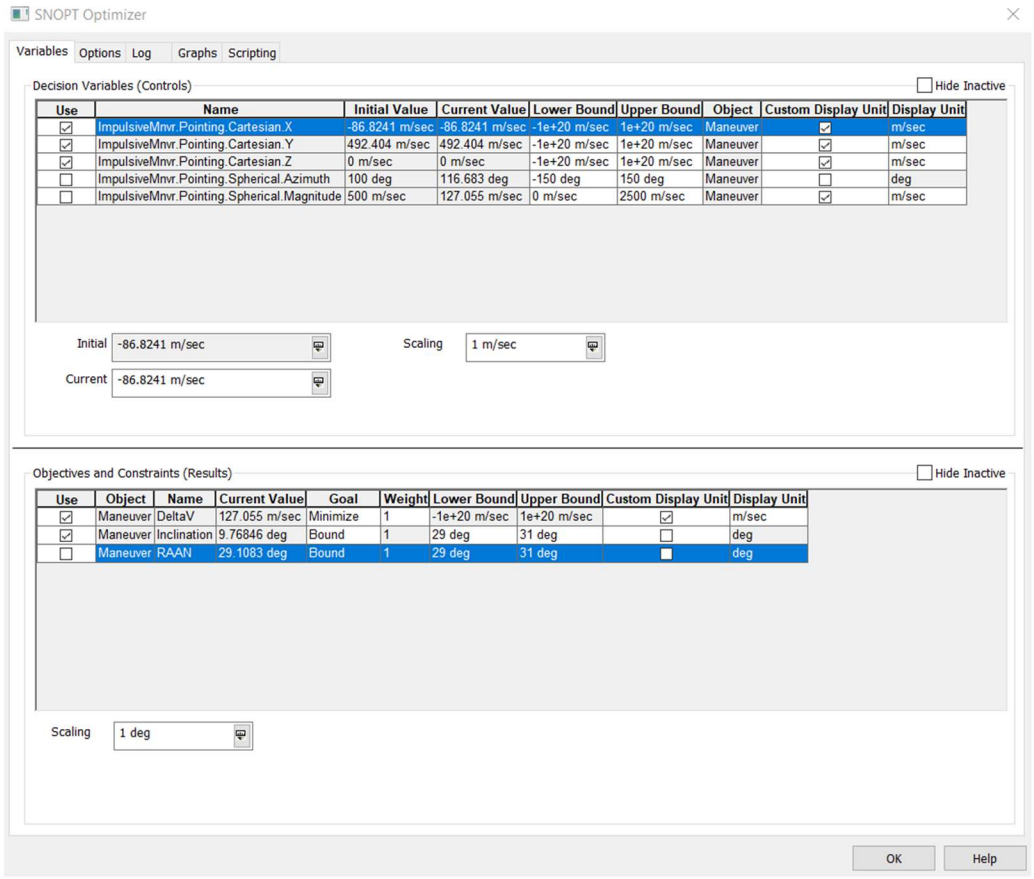

Figure 17: SNOPT profile of the "Inclination change" targeting sequence from Fig. 20. Note the RAAN target constraint is is turned off. As a precaution, the maneuver to target the inclination was always set to minimize ΔV. Since the inclination change would be instantaneous the duration of this maneuver cannot be minimized.

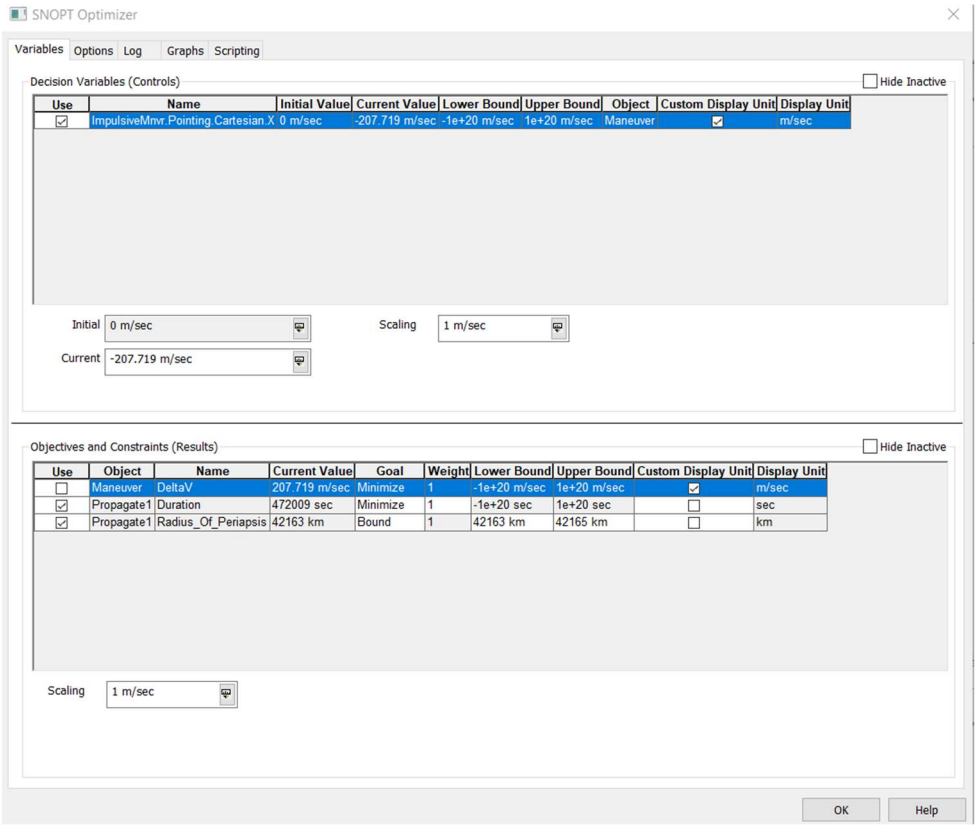

Figure 18: SNOPT profile of the "Lower orbit" targeting sequence. Note that the duration of the propagate segment is checked and set to minimize. This is what minimizes the TOF of the trajectory. To minimize the ΔV of the trajectory, the ΔV constraint of the maneuver object would need to be checked.

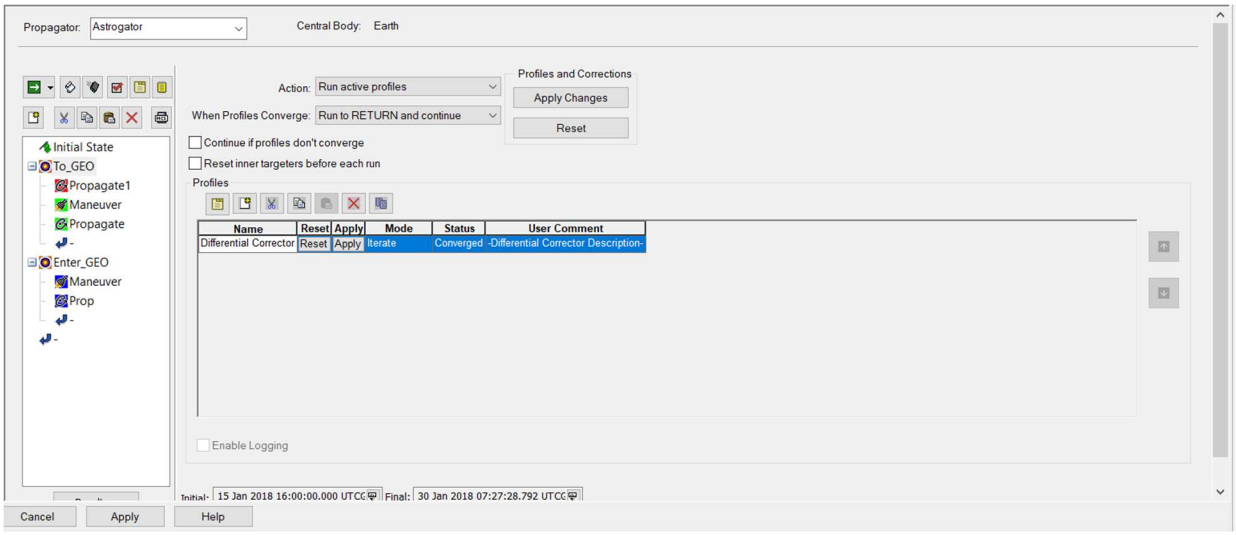

Figure 19: Targeting profile of the DPO to GEO trajectory. Note the use of only the differential corrector with the targeting sequence. Within the targeting sequence "To Geo" the portion of the DPO is included.

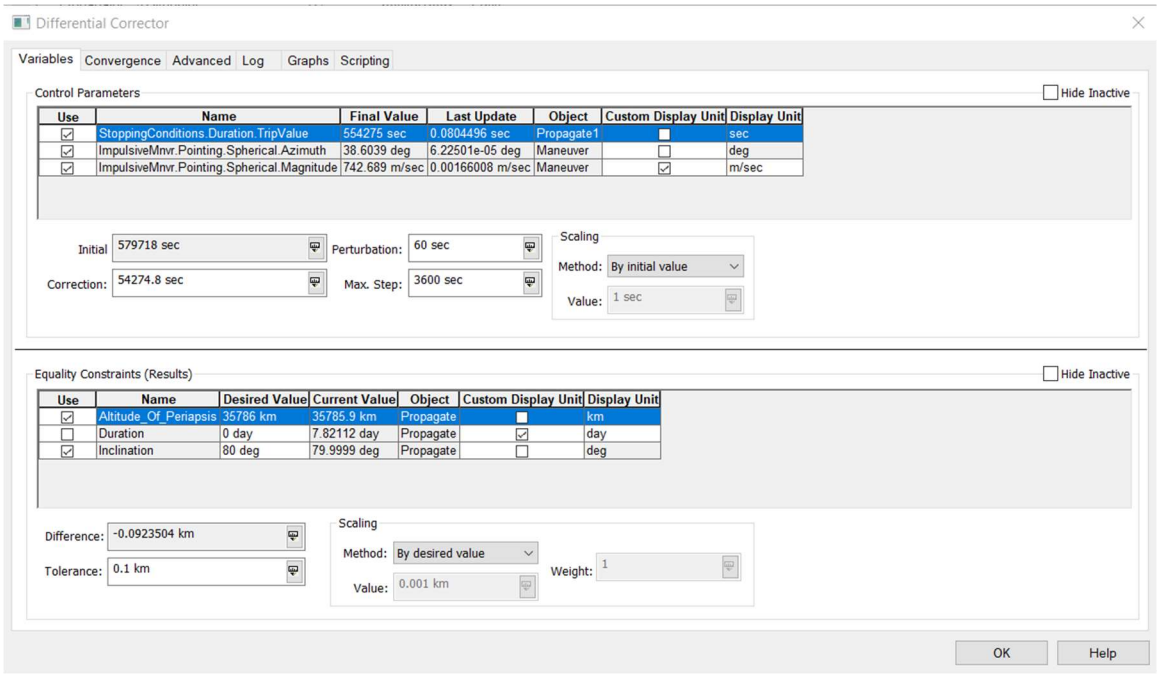

Figure 20: Differential corrector profile to "To GEO" target sequence in Fig. 23.

The initial conditions found by this differential corrector could not be applied to the SNOPT to find optimal trajectories from the DPO to GEO. Note that the trajectory cannot be optimized within the differential corrector. Setting the desired duration of the propagate segment to zero will not minimize the duration.

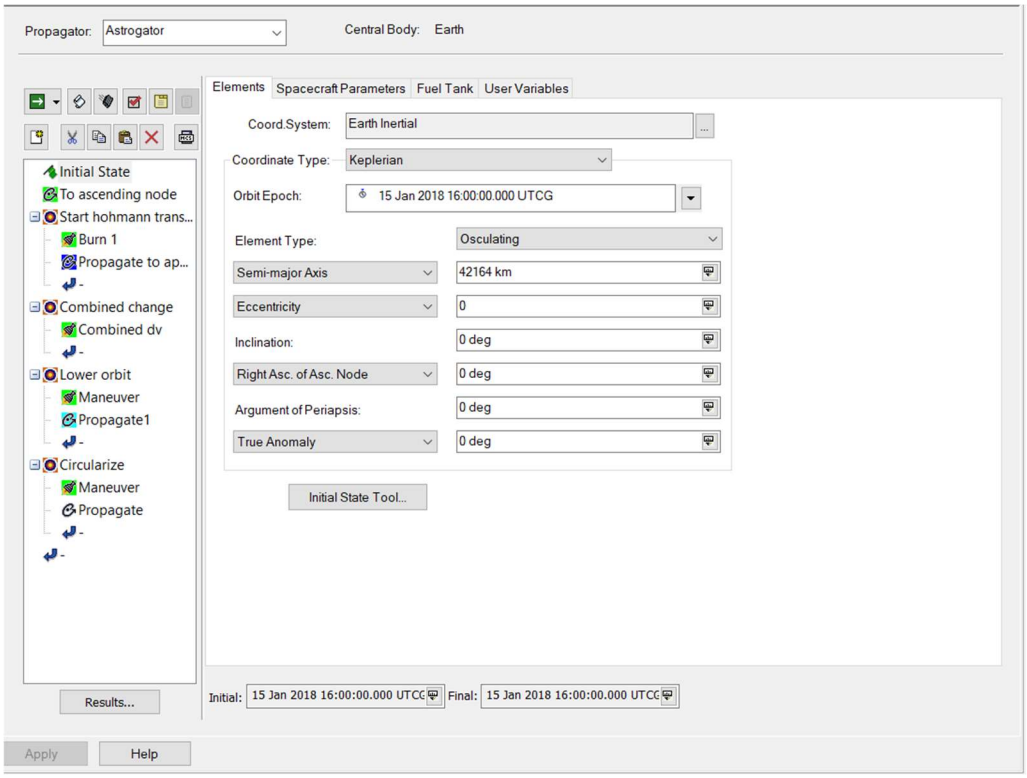

Figure 21: Targeting profile of inclination change using Hohmann transfer to a greater radius of GEO. Modified strategy from STK tutorial.

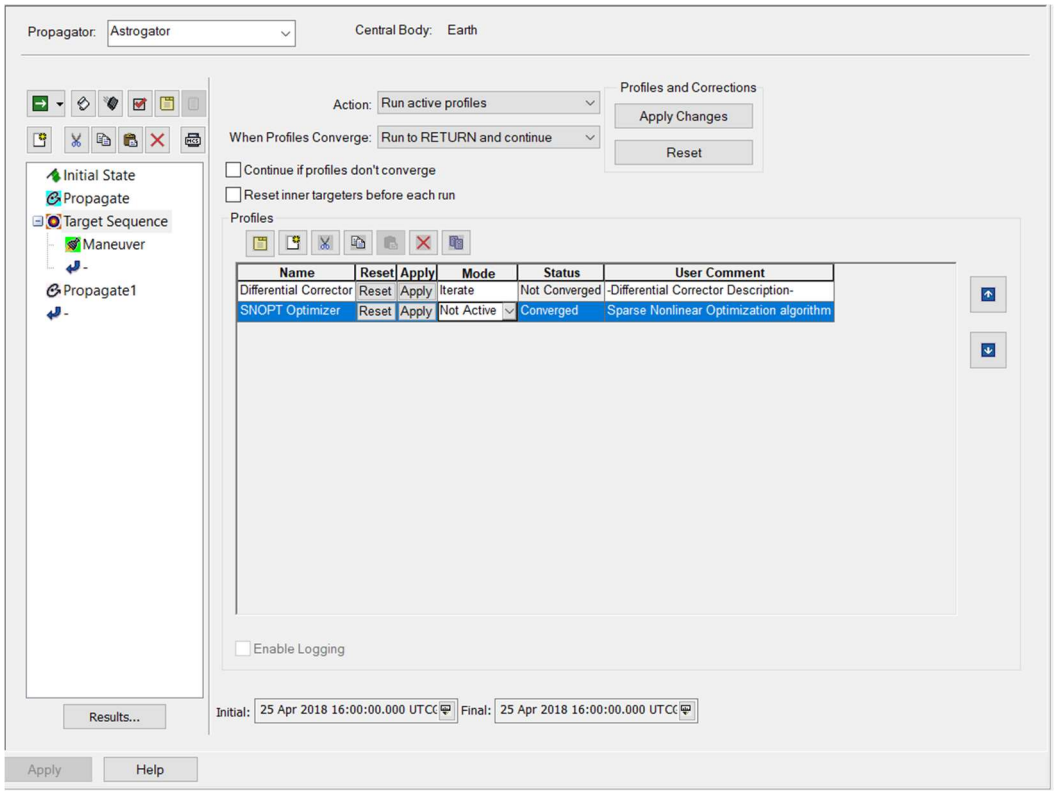

Figure 22: Targeting profile of inclination change done at GEO. Note that the differential corrector and SNOPT were used to test if the ΔV of the maneuver could be minimized. No difference was found, and the differential corrector was used for the inclination changes.

Appendix B

This appendix attempts to capture some of the limitations of the software used in this investigation. The software used by the investigation was Analytical Graphics Inc.'s (AGI's) Systems Toolkit (STK) software. This software was used to model the trajectories from an L_1 Lyapunov orbit (L_1) to geosynchronous orbit (GEO), trajectories from a distant prograde orbit (DPO) to GEO, and various inclination changes between GEOs. STK provided not only visual models, but the data on ΔV and time-of-flight (TOF) as well. The sparse nonlinear optimizer (SNOPT) was used within STK to minimize either the ΔV cost of TOF parameters of the trajectories and therefore attain the optimal trajectories.

An issue when collecting data was that when the SNOPT attempted to minimize TOF it would sometimes generate unrealistic trajectories. The optimal trajectory selected by the SNOPT would be the extreme solution and provide a TOF on the order of just a few seconds and therefore a relativistic speed, see Fig. 23-24. However, by just adjusting the thrust parameters of the impulsive maneuver within the targeting sequence and adjusting the bounds of the inclination targeted by the SNOPT, this issue could often be remedied.

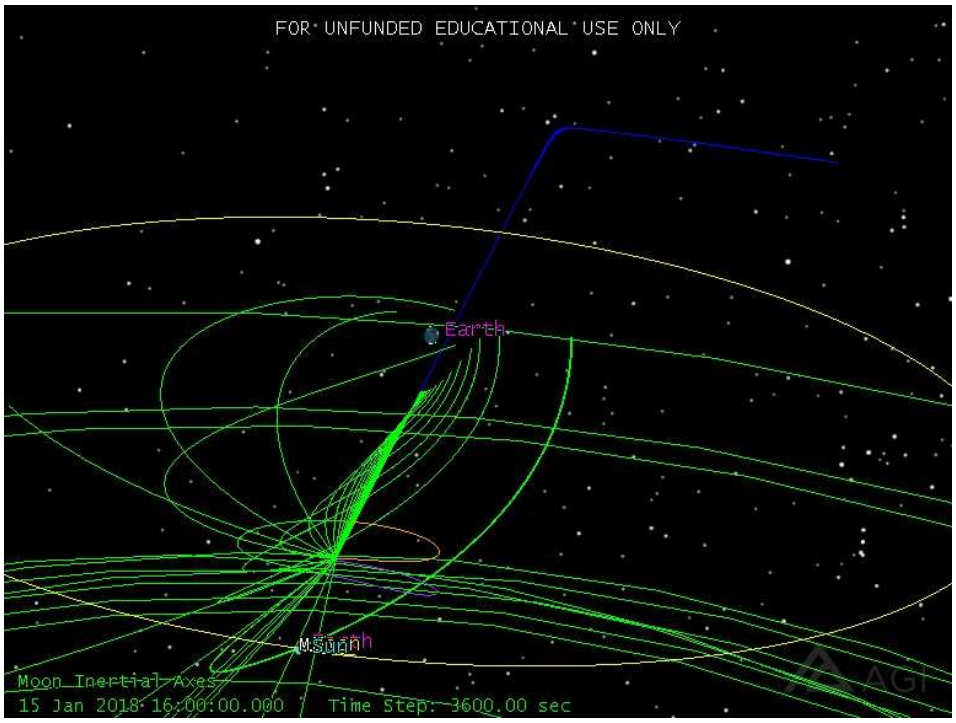

Figure 23: Example of TOF-minimized trajectory where the SNOPT has selected a relativistic solution.

Control	Current Value	Last Update		Result	Goal	Current Value	Status
...iveMnvr.Pointing.Cartesian.X	-4016226.9609 m/sec	-2.95927748084e-06		Propagate1 : Duration	Minimize	9.74939932326 sec	------
...veMnvr.Pointing.Cartesian.Y	610931.743324 m/sec	-2.05861870199e-05		... : Radius_Of_Periapsis	Bound	42163 km	In bounds
...iveMnvr.Pointing.Cartesian.Z	-33660887.4537 m/se	-4507.28174963 m/se					

Figure 24: Screen capture of the SNOPT outputs from the trajectory displayed in Fig. 23. The SNOPT minimized the TOF between L_1 and GEO to just 9.75 seconds.

Other times, when minimizing ΔV the SNOPT would give trajectories that appeared to possibly use the invariant manifolds in some cases and would take hundreds of days if they even connected to GEO. These results were ultimately tossed as they occurred seemingly randomly, and it was simply remedied by shifting the thrust parameters. However, not all trajectories did connect with GEO and often times went far out of the Earth-Moon system despite the SNOPT finding some solutions which came

very close to being feasible, see Fig. 25-26. This problem appears to have been caused by the RAAN selection criteria. As can be seen in Fig. 18, the trajectories nearly reaching GEO appear to be opposite each other in RAAN while still targeting the same inclination. However, it is not clear why this led to such large and indirect trajectories.

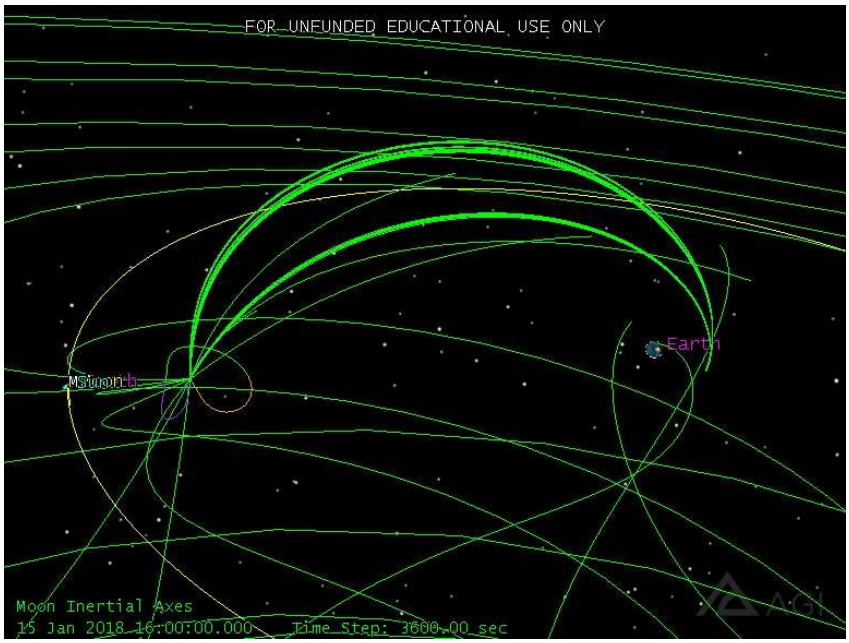

Figure 25: Example of SNOPT finding a large number of nearly-feasible solutions, but also searching far outside of the system. Note the trajectories approaching GEO come in at opposite RAANs despite targeting the same inclination. This realization led to the RAAN parameter being dropped from the investigation.

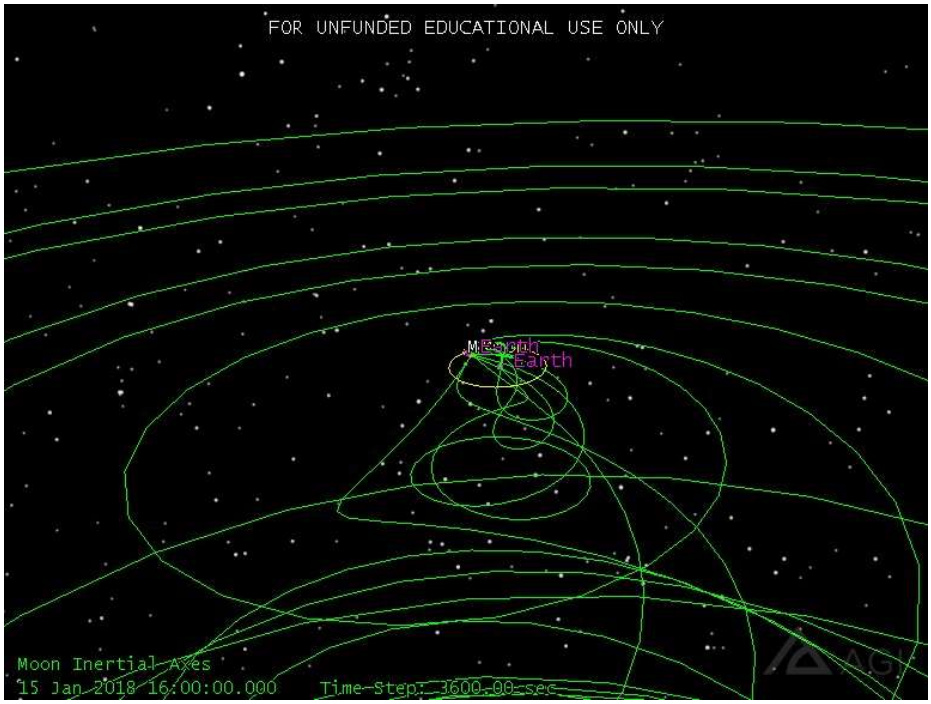

Figure 26: Same screen capture as Fig. 18, but from a greater distance from the Earth-Moon system (yellow circle is the Moon's orbit about the Earth), showing the size of some of the trajectories the SNOPT searched through.

Another issue with software which effected the investigation, was the inability to easily shift the scenario epoch. This issue ultimately led to dropping the dynamic portion of the investigation. No resources could be found on how to shift the entire scenario to a different starting time. The only evident way seemed to be to recreate the entire scenario—which includes not only the trajectories, but also the frames of reference and custom axes needed to create the Lagrange point orbits—in another file at a different starting time. To get any meaningful results this process would have to be repeated several times to determine if the location of the Moon within its orbit has an effect on the ΔV and TOF costs of the trajectories.

Bibliography

[1] S. Chakrabarti, “How many satellites are orbiting Earth?,” Sep. 25, 2021. https://www.space.com/how-many-satellites-are-orbiting-earth (accessed Jan. 10, 2022).

[2] D. J. Trump, *Memorandum on Space Policy Directive 7* . The White House, 2021.

[3] S. Erwin, “Air Force: SSA is no more; it’s ’Space Domain Awareness’ - SpaceNews,” *Space News*, Nov. 14, 2019.

[4] S. Young, “The Number of Active Satellites in Space Skyrockets . . . Literally,” *Union of Concerned Scientists*, Jul. 27, 2021. https://allthingsnuclear.org/syoung/number-of-satellites-skyrockets/ (accessed Jan. 20, 2022).

[5] “Annual Threat Assessment of the US Intelligence Community,” Washington D.C., 2021.

[6] “United States Space Priorities Framework,” 1 December. The White House, Washington D.C., 2021, [Online]. Available: https://www.whitehouse.gov/wp-content/uploads/2021/12/United-States-Space-Priorities-Framework-_-December-1-2021.pdf.

[7] J. Foust, “Russia destroys satellite in ASAT test ,” *SpaceNews*, Nov. 15, 2021. https://spacenews.com/russia-destroys-satellite-in-asat-test/ (accessed Jan. 10, 2022).

[8] M. Garcia, “Space Debris and Human Spacecraft,” May 27, 2021. http://www.nasa.gov/mission_pages/station/news/orbital_debris.html (accessed Jan. 28, 2022).

[9] S. Erwin, “Debris removal a key goal in Space Force’s ‘Orbital Prime’ project - SpaceNews,” *Space News*, Nov. 04, 2021.

[10] “Northrop Grumman and Intelsat Make History with Docking of Second Mission Extension Vehicle to Extend Life of Satellite,” *Northrop Grumman*, Apr. 12, 2021. https://news.northropgrumman.com/news/releases/northrop-grumman-and-intelsat-make-history-with-docking-of-second-mission-extension-vehicle-to-extend-life-of-satellite (accessed Jan. 10, 2022).

[11] A. R. Collins and K. W. Johnson, “Development of cislunar space logistics networks for satellite constellation support using event-driven generalized multi-commodity network flows,” *AIAA Scitech 2020 Forum*, vol. 1 PartF, 2020, doi: 10.2514/6.2020-2135.

[12] W. E. Wiesel, *Modern Orbit Determination*. Beavercreek, Ohio: Aphelion Press, 2010.

[13] J. A. Ostman, “Cislunar Trajectory Generation with Sun-Exclusion Zone Constraints Using a Genetic Algorithm and Direct Method Hybridization,” *Theses Diss.*, vol. 2373, 2019, [Online]. Available: https://scholar.afit.edu/etd/2373/.

[14] T. A. Pavlak, “Trajectory Design and Orbit Maintenance Strategies in Multi- Body Dynamical Regimes,” Purdue University, 2013.

[15] L. L. Euler, “De motu rectilineo trium corporum se mutuo attrahentium,” *Novi Comment. Acad. Sci. Petropolitanae*, vol. 11, pp. 144–151, 1767, Accessed: Aug. 08, 2021. [Online]. Available: https://scholarlycommons.pacific.edu/euler-works/327.

[16] M. J. Holzinger, C. C. Chow, and P. Garretson, “A Primer on Cislunar Space,” 2021. Accessed: Jul. 12, 2021. [Online]. Available: https://www.afrl.af.mil/Portals/90/Documents/RV/A Primer on Cislunar Space_Dist A_PA2021-1271.pdf?ver=vs6e0sE4PuJ51QC-15DEfg%3D%3D.

[17] E. M. Zimovan-Spreen, K. C. Howell, and D. C. Davis, “Near rectilinear halo orbits and nearby higher-period dynamical structures: orbital stability and resonance properties,” *Celest. Mech. Dyn. Astron.*, vol. 132, no. 5, pp. 1–25, 2020, doi: 10.1007/s10569-020-09968-2.

[18] B. B. Jagannatha and K. Ho, “Event-Driven Network Model for Space Mission Optimization with High-Thrust and Low-Thrust Spacecraft,” *J. Spacecr. Rockets*, vol. 57, no. 3, pp. 446–463, 2020, doi: 10.2514/1.A34628.

[19] R. Whitley and R. Martinez, “Options for staging orbits in cislunar space,” in *IEEE Aerospace Conference Proceedings*, 2016, vol. 2016-June, doi: 10.1109/AERO.2016.7500635.

[20] J. N. Brick, “Military Space Mission Design and Analysis in a Multi-Body Environment: An Investigation of High-Altitude Orbits as Alternative Transfer Paths, Parking Orbits for Reconstitution, and Unconventional Mission Orbits,” Air Force Institute of Technology, 2017.

[21] S. R. Knister, “Evaluation Framework for Cislunar Space Domain Awareness (SDA) Systems,” Air Force Institute of Technology, 2019.

[22] J. S. Parker and R. L. Anderson, *Low-Energy Lunar Trajectory Design*, vol. 9781118853, no. July. Pasadena, CA: Jet Propulsion Laboratory, 2013.

[23] D. Chongrui, M. K. Fain, and O. L. Starinova, “Analysis and design of halo orbits in cislunar space,” *IOP Conf. Ser. Mater. Sci. Eng.*, vol. 984, no. 1, 2020, doi: 10.1088/1757-899X/984/1/012033.

[24] G. Lantoine, “Efficient NRHO to DRO Transfers in Cislunar Space,” in *Advances in the Astronautical Sciences*, 2017, vol. 162, pp. 2565–2582, [Online]. Available: http://hdl.handle.net/2014/47543.

[25] R. J. Whitley *et al.*, “Earth-moon near rectilinear halo and butterfly orbits for lunar surface exploration,” *Adv. Astronaut. Sci.*, vol. 167, no. November 2020, pp. 3873–3892, 2018.

[26] L. Capdevila, D. Guzzetti, and K. Howell, “Various transfer options from Earth into Distant Retrograde Orbits in the vicinity of the Moon,” in *AAS/AIAA Space Flight Mechanics Meeting*, 2014, vol. 118.

[27] L. R. Capdevila and K. C. Howell, “A transfer network linking Earth, Moon, and the triangular libration point regions in the Earth-Moon system,” *Adv. Sp. Res.*, vol. 62, no. 7, pp. 1826–1852, 2018, doi: 10.1016/j.asr.2018.06.045.

[28] C. Bezrouk and J. Parker, “Long Duration Stability of Distant Retrograde Orbits,” no. August, pp. 1–9, 2014, doi: 10.2514/6.2014-4424.

[29] G. Mingotti, F. Topputo, and F. Bernelli-Zazzera, “Transfers to distant periodic orbits around the Moon via their invariant manifolds,” *Acta Astronaut.*, vol. 79, pp. 20–32, Oct. 2012, doi: 10.1016/J.ACTAASTRO.2012.04.022.

[30] W. Anthony, A. Larsen, E. A. Butcher, and J. S. Parker, “Impulsive guidance for optimal manifold-based transfers to earth-moon L1 halo orbits,” in *Advances in the Astronautical Sciences*, 2014, vol. 150, pp. 761–777, Accessed: Aug. 25, 2021. [Online]. Available: https://www.researchgate.net/publication/289023514.

[31] D. Lee, E. A. Butcher, and A. K. Sanyal, “Optimal interior Earth-Moon Lagrange point transfer trajectories using mixed impulsive and continuous thrust,” *Aerosp. Sci. Technol.*, vol. 39, pp. 281–292, 2014, doi: 10.1016/j.ast.2014.09.016.

[32] N. L. O. Parrish, “Low Thrust Trajectory Optimization in Cislunar and Translunar Space,” 2018.

[33] L. Maodeng and J. Wuxing, “Translunar low-energy trajectories via Earth-Moon L1 Lyapunov orbit,” in *2007 IEEE International Conference on Robotics and Biomimetics, ROBIO*, 2007, no. 60535010, pp. 941–945, doi: 10.1109/ROBIO.2007.4522290.

[34] Q. Qu, M. Xu, and K. Peng, “The cislunar low-thrust trajectories via the libration point,” *Astrophys. Space Sci.*, vol. 362, no. 5, pp. 1–11, 2017, doi: 10.1007/s10509-017-3075-2.

[35] T. Ishimatsu, “Generalized Multi-Commodity Network Flows: Case Studies in Space Logistics and Complex Infrastructure Systems,” Massachusetts Institute of Technology, 2013.

[36] S. C. Dimri and M. Ram, “Flow Maximization Problem as Linear Programming Problem with Capacity Constraints,” vol. 13, no. 1, pp. 508–515, 2018, [Online]. Available: http://pvamu.edu/aam.

[37] A. Itai, “Two-Commodity Flow,” *J. ACM*, vol. 25, no. 4, pp. 596–611, 1978, doi: 10.1145/322092.322100.

[38] T. Ishimatsu, O. L. De Weck, J. A. Hoffman, and Y. Ohkami, “Generalized multicommodity network flow model for the earth-moon-mars logistics system,” *J. Spacecr. Rockets*, vol. 53, no. 1, pp. 25–38, 2016, doi: 10.2514/1.A33235.

[39] B. Jagannatha and K. Ho, “Event-Driven Space Logistics Network Optimization with Embedded Propulsion Technology Trades,” pp. 1–35, 2019, [Online]. Available: http://arxiv.org/abs/1904.09364.

[40] K. Ho, O. L. De Weck, J. A. Hoffman, and R. Shishko, “Dynamic modeling and optimization for space logistics using time-expanded networks,” *Acta Astronaut.*, vol. 105, no. 2, pp. 428–443, 2014, doi: 10.1016/j.actaastro.2014.10.026.

[41] R. T. Nallapu, L. D. Vance, Y. Xu, and J. Thangavelatham, “Automated Design Architecture for Lunar Constellations,” *IEEE Aerosp. Conf. Proc.*, 2020, doi: 10.1109/AERO47225.2020.9172381.

[42] G. Sowers, “Thermal Mining of Ices on Cold Solar System Bodies. NIAC Phase I Finland Report,” no. February, 2020, [Online]. Available: https://www.nasa.gov/directorates/spacetech/niac/2019_Phase_I_Phase_II/Thermal_Mining_of_Ices_on_Cold_Solar_System_Bodies/.

[43] N. M. Curran, M. Nottingham, L. Alexander, I. A. Crawford, E. Füri, and K. H. Joy, “A database of noble gases in lunar samples in preparation for mass spectrometry on the Moon,” *Planet. Space Sci.*, vol. 182, p. 104823, Mar. 2020, doi: 10.1016/J.PSS.2019.104823.

[44] B. Cheetham, T. Gardner, and A. Forsman, “Cislunar autonomous positioning system technology operations and navigation experiment (Capstone),” *Accel. Sp. Commer. Explor. New Discov. Conf. ASCEND 2020*, pp. 1–8, 2020, doi: 10.2514/6.2020-4140.

[45] S. Erwin, “Air Force Research Laboratory announces new space experiments - SpaceNews,” *SpaceNews.com*, Sep. 02, 2020. https://spacenews.com/air-force-research-laboratory-announces-new-space-experiments/ (accessed Aug. 31, 2021).

[46] A. Jones and L. C. Rabelo, “Survey of Job Shop Scheduling Techniques.”

[47] R. Cheng, M. Gen, and Y. Tsujimura, “A tutorial survey of job-shop scheduling problems using genetic algorithms—I. representation,” *Comput. Ind. Eng.*, vol. 30, no. 4, pp. 983–997, Sep. 1996, doi: 10.1016/0360-8352(96)00047-2.

[48] L. Barbulescu, A. Howe, and D. Whitley, “AFSCN scheduling: How the problem and solution have evolved,” *Math. Comput. Model.*, vol. 43, no. 9–10, pp. 1023–1037, May 2006, doi: 10.1016/j.mcm.2005.12.004.

[49] Q. Zhang, H. Manier, and M. A. Manier, “A genetic algorithm with tabu search procedure for flexible job shop scheduling with transportation constraints and bounded processing times,” *Comput. Oper. Res.*, vol. 39, no. 7, pp. 1713–1723, Jul. 2012, doi: 10.1016/j.cor.2011.10.007.

[50] C.-H. Liu and C.-I. Hsu, “Dynamic job shop scheduling with fixed interval deliveries,” *Prod. Eng.*, vol. 9, no. 3, pp. 377–391, 2015, doi: 10.1007/s11740-015-0605-z.

[51] D. A. Vallado, “Coplanar Maneuvers,” in *Fundamentals of Astrodynamics and Applications*, 4th ed., J. Wertz, Ed. Hawthorne, CA: Microcosm Press, 2013, pp. 320–328.

[52] D. A. Vallado, “Noncoplanar Transfers,” in *Fundamentals of Astrodynamics and Applications*, 4th ed., J. Wertz, Ed. Hawthorne, CA: Microcosm Press, 2013, pp. 337–345.

[53] D. Kornuta *et al.*, “Commercial lunar propellant architecture : A collaborative study of lunar propellant production ☆,” *Reach - Rev. Hum. Sp. Explor.*, vol. 13, no. November 2018, p. 100026, 2019, doi: 10.1016/j.reach.2019.100026.

[54] J. A. Dahlke, “Optimal Trajectory Generation in a Dynamic Multi-Body Environment Using a Pseudospectral Method,” 2018.

REPORT DOCUMENTATION PAGE

Form Approved
OMB No. 074-0188

1. REPORT DATE *(DD-MM-YYYY)*	2. REPORT TYPE	3. DATES COVERED *(From – To)*
24-03-2022	Master's Thesis	October 2020 – March 2022

ITLE AND SUBTITLE

Development of Minimum Delta-V Trajectories to Service GEO Assets from Cislunar Space

5a. CONTRACT NUMBER

5b. GRANT NUMBER

5c. PROGRAM ELEMENT NUMBER

6. AUTHOR(S)

Urban, Alexander C., 2nd Lt, USAF

5d. PROJECT NUMBER

5e. TASK NUMBER

5f. WORK UNIT NUMBER

7. PERFORMING ORGANIZATION NAMES(S) AND ADDRESS(S)
Air Force Institute of Technology
Graduate School of Engineering and Management (AFIT/EN)
2950 Hobson Way, Building 640
WPAFB OH 45433-7765

8. PERFORMING ORGANIZATION REPORT NUMBER

AFIT-ENY-MS-22-M-315

9. SPONSORING/MONITORING AGENCY NAME(S) AND ADDRESS(ES)
AGENCY: Air Force Research Laboratoy Space Vehicles Directorate
ADDRESS: 3550 Aberdeen Drive SE
Kirtland AFB, NM 87117
PHONE and EMAIL: (505) 853-3088 karl.stolleis@spaceforce.mil
ATTN: Karl Stolleis

10. SPONSOR/MONITOR'S ACRONYM(S)

AFRL/RVSV

11. SPONSOR/MONITOR'S REPORT NUMBER(S)

12. DISTRIBUTION/AVAILABILITY STATEMENT
DISTRUBTION STATEMENT A. APPROVED FOR PUBLIC RELEASE; DISTRIBUTION UNLIMITED.

13. SUPPLEMENTARY NOTES
This material is declared a work of the U.S. Government and is not subject to copyright protection in the United States.

14. ABSTRACT
Orbits around Earth are becoming increasingly congested and contested, posing potential future threats to space assets. Cislunar space may offer an effective solution to these problems by offering storage for servicing and replacement vehicles. This investigation explores how to minimize the dV costs required of a network of service vehicles traveling from cislunar space to GEO using in-situ resource utilization. In this investigation the arc costs of an event-driven generalized multicommodity network flow are generated for creation of a model to be used to develop a dynamic scheduler. High-thrust trajectories between various inclinations of GEO, an Earth-Moon L1 Lyapunov orbit (L1), and a distant prograde orbit (DPO) are used. The effect of orbit radius on minimizing dV of inclination changes in GEO is also investigated to determine arc costs for multiple deliveries within GEO. It was found that there is little variation in time-of-flight in trajectories leaving L1, but significant variation in dV costs. DPO trajectories also appear to offer significant dV savings in comparison to L1 trajectories. In GEO, dV costs of inclination changes are minimized either at GEO radius (42,164 km) or at a multiple of 1.25xGEO radius (52,75 km).

15. SUBJECT TERMS
Cislunar, Event-Driven Generalized Multicommodity Network Flow, Scheduling, Inclination Changes

16. SECURITY CLASSIFICATION OF:			17. LIMITATION OF ABSTRACT	18. NUMBER OF PAGES	19a. NAME OF RESPONSIBLE PERSON
a. REPORT	b. ABSTRACT	c. THIS PAGE			Dr. Bruce Cox, AFIT/ENS
U	U	U	UU	110	19b. TELEPHONE NUMBER *(Include area code)* (937) 255-3636, ext 4377 (bruce.cox@afit.edu)

Standard Form 298 (Rev. 8-98)
Prescribed by ANSI Std. Z39-18